
# Holistic Multi-Parametric Magnetic Resonance Image Processing for Identification of Neoplasm and normal Brain Tissues

**By**

**Teferi Chernet Woldetekle**

**A thesis Submitted in Partial Fulfillment of the Requirements for the Degree of Master of Science in Biomedical Engineering (Bio-Instrumentation and Imaging Stream)**

**CENTER OF BIOMEDICAL ENGINEERING**

**ADDIS ABABA INSTITUTE OF TECHNOLOGY**

**SCHOOL OF GRADUATE STUDIES**

**ADDIS ABABA UNIVERSITY**

**Advisors: Dawit Assefa Haile (PhD.)**

**Birhanu Assefa (MSc.)**

**Addis Ababa, Ethiopia, December 2016**

# Declaration

I, the undersigned, declare that this thesis is my original work. It has never been presented for a degree in any other institution and that all sources of materials used in it have been duly acknowledged.

Name: Teferi Chernet Woldetekle

Signature: _____

Place: Addis Ababa

Date of submission: _____

This thesis work has been submitted for examination with my approval as advisor.

Dawit Assefa Haile (PhD.) _____

Advisor's Name Signature

# Addis Ababa University

# School of Graduate Studies

## Certificate of Examination

This is to certify that the thesis prepared by Teferi Chernet Woldetekle entitled: ***Holistic Multi-Parametric Magnetic Resonance Image Processing for use in Cancer Tumor Identification*** submitted in partial fulfillment of the requirements for the degree of Master of Science in Biomedical Engineering (Bioinstrumentation and Imaging) complies with the regulations of the University and meets the accepted standards with respect to originality and quality.

Signed by the examining committee

Examiner_____Signature_____Date_____

Examiner_____Signature_____Date_____

Examiner_____Signature_____Date _____

Advisor_____Signature_____Date_____

_____

Chief of Department or Graduate program coordinator

# Abstract

A breakthrough advance in Magnetic Resonance Imaging (MRI) into standard clinical practices has enabled greater accuracy in delineating tumor volumes. The technique allows autonomous detection through noninvasive imaging of malignant brain tumors like gliomas and similar other body tumors for the requirement of efficient and effective procedures like biopsy and radiation therapy as well as for quantification of patients' responses to treatment.

The role of MR imaging in regard of characterization schemes of neoplasms has been tremendous. There are many approaches suggested in the literature for this purpose, one of which is color processing concept.

Most color images have three components and each pixel/voxel on such color images can be represented as a three-component vector. Analogously, an MRI voxel, for example, can be seen as a vector with as many channels as available MR image parameters: T1, T2, PD, ADC, rCBV, Ktrans, T2*, etc. and there can be various methods of representing such images as colors.

Hence using these methodologies and by combining multiple MRI parameters as we need, we can maximize the information we want to display. The research study exploits advanced mathematical and image analysis assets for use in analysis of MP-MR medical images making use of algorithmic procedures. Accuracy and potentials of the method is compared against gold standards (available ground truth). The data used is composed of standard co-registered multiple MR image parameters taken from patients treated for the highest grade and most aggressive of the gliomas. This approach comes with a great potential to assist accurate and effective detection, visualization, and analysis of useful medical image information for physicians and/or researchers as well.

Even though MR images are the subjects of interest in this study, in principle the method developed could be applied to other medical images with multiple components acquired through different modalities.



***Keywords: Quaternion Fourier Transform, Trinion Fourier Transform, Image Processing, Principal Component Analysis.***

# Acknowledgement

I would like to seize this moment to share my sincere gratitude to those who supported and encouraged me throughout the development of this work. First of all, I would like to acknowledge my senior advisor, Dr. Dawit Assefa Haile (PhD) who supervised, guided and constantly keeping me on track, for all his help in writing up and editing the literature, providing me knowledge, suggestions and invaluable feedback that made this thesis possible. I would like to thank my co-advisor Mr. Birhanu Assefa (MSc.) for his technical suggestions and honest assessment of the performance of my methods, for providing me with corrections related to this work. I would like to thank Dr. Masreshaw Demelash (PhD.), PG coordinator, for all his continuous follow-ups, help and encouragement.

My thanks also go to Dr. Guta Zenebe (Neuro-oncologist and owner of Yehulushet H. Clinic) and Dr. Mihila Zebenigus (Neuro-oncologist and Medical Director of this clinic) for sharing their medical expertise and interest in this work, without which this work could not have succeeded.

I would like to thank everyone else who has ever made suggestions related to my work and helped me on data collection. This list includes Berihun Gebrehawaryat, Desta Bekele and Samuel Getaneh who all have been there both in the work and leisure, making this degree an unforgettable experience.

Special thanks to my family namely my mother Fikirte Wube, brothers Terefe Chernet and Shiferaw Chernet for their love, comprehension and wisdom that accompanied me in every moment. And last but not least, I would like to thank my intimate friend Mr. Mihiret Tesfaye (MSc.) for all his love and encouragement, guidance and counseling.

# Table of content

# List of Tables

# List of Figures

# Abbreviations and Acronyms

| | |
|---|---|
| 2D | Bi-Dimensional |
| 3D | 3-dimensional |
| ADC | Apparent Diffusion Coefficient |
| BBB | Blood Brain Barrier |
| CSF | Cerebro-Spinal Fluid |
| CT | Computed Tomography |
| DICOM | Digital Imaging and Communications in Medicine |
| DTPA | Diethyl Triamine Penta-Acetic |
| DWI | Diffusion-Weighted Imaging |
| EPI | Echo Planar Imaging |
| FLAIR | Fluid Attenuated Inversion Recovery |
| FSE | Fast Spin Echo |
| FSPGR | Fast Spoiled Gradient Echo |
| GBM | Glioblastoma Multiforme |
| Gd | Gadolinium |
| GRE | Gradient Echo Pulse Sequence |
| GTV | Grose Tumor Volume |
| MPMRI | Multi-Parametric Magnetic Resonance Imaging |
| MRI | Magnetic Resonance Imaging |
| PET | Positron Emission Tomography |
| rCBV | Relative Cerebral Blood Volume |
| RF | Radio Frequency |
| ROI | Region of Interest |
| SNR | Signal to noise ratio |
| T | Tesla |
| T1 | Spin-lattice (longitudinal) relaxation time |
| T2 | Spin-spin (transverse) relaxation time |
| TE | Echo Time |
| TR | Repetition Time |
| YCbCr | is a family of color spaces used as a part of the color image pipeline |

in video and digital photography systems. Y is the luma component and CB and CR are the blue-difference and red-difference Chroma components respectively.

# CHAPTER 1. Introduction

## 1.1. Background

Advances in medical imaging technology today enable the construction of complex autonomous tumor detector systems. Magnetic resonance imaging (MRI), nuclear magnetic resonance imaging (NMRI), or magnetic resonance tomography (MRT) is a medical imaging technique used in radiology to investigate the anatomy and physiology of the human body in both health and disease statuses. The technique is widely used in hospitals for medical diagnosis, staging of disease and for follow-up. There has been a 10% annual growth in MR usage over the last decade or so [3] and, although the technique avoids ionizing radiation, there are concerns about cost effectiveness and over diagnosis.

MRI is a versatile tool for the non-invasive assessment of medical images specially in brain anatomy and function and has several important clinical and research applications, but might not yet have reached its full potential. There is always a demand for better and accurate medical images for better tumor detection. A variety of imaging techniques are used to study brain tumors, including MRI, computed tomography (CT), single photon emission computed tomography (SPECT), positron emission tomography (PET), and cerebral angiography. SPECT and PET imaging serve smaller roles, although their ability to provide information on tissue biology and physiology can be greatly helpful. PET scanning is also used to evaluate tumor grades [49].

At this moment, CT and MR imaging are the most widely used techniques, because of their widespread availability and their ability to produce high resolution images of normal anatomic structures and pathological tissues [48]. CT is best suited for viewing bone injuries, diagnosing lung and chest problems, and detecting cancers. MRI is suited for examining soft tissue in ligament and tendon injuries, spinal cord injuries, brain tumors, etc. Whereas CT is the fastest modality, making it the preferred examination for imaging critically ill or medically unstable patients, widely used in emergency rooms because the scan takes fewer than 5 minutes. An MRI, on the other hand, can take up to 30 minutes and typically costs

much more than a CT scan. One advantage of an MRI is that it does not use radiation while CT scanners do. This radiation is harmful if there is repeated exposure [48].

MRI has become the driving force for technology development in every aspect in image processing system since it offers greater flexibility, efficiency, and superior soft-tissue contrast and hence has been used in various applications such as in identification of diseases, tissue classification, as well as segmentation. Current state-of-the-art MRI technologies embrace several innovative ideas particularly for use in cancer research [36]. Hence MRI is a powerful, non-invasive medical technology that allows physicians to better identify and study pathologies in biological tissues. The tissues examined can be represented as sectional images (axial/transvers, coronal, or sagittal) showing great contrast between healthy and stressed tissue with high resolution while the MR signals from various tissue segments are displayed as video pixels. Hence our focus is on the conceptual overview of the principles of MRI on anatomic and functional modalities being, one of the major modern imaging expertises currently in use [39].

Over the years, MRI has become a popular and widely available means of cross sectional imaging modality. That is not coincidental; MRI has gone through a fast-paced round of development since its discovery. Now every self-respecting hospital or clinic should have to have one or more MRI scanners to battle the conquest for more precise and accurate imaging and diagnosis of pathology. Paired with its excellent image contrast resolution, MRI is harmless to the human body, within reason, through its use of radio waves and a magnetic field. This is in contrast with X-ray and CT examinations, which use ionizing radiation [29].

Through the years, operation of MRI scanners has become easier with each new software release, but this does not eliminate the need for proper understanding of how MRI works. MRI works with a host of parameters, such as T1, T2, TR, TE, PD and ADC to name but a few. A thorough understanding of these parameters is vitally important in order to produce a successful MR image [7].

MR imaging is one of the most powerful and harmless ways to study human inner tissues. It gives the chance of having an accurate insight into the physiological conditions of the human body, and specially, the brain [10]. Conventional MR imaging is the standard technique for diagnosis, treatment planning, and monitoring of Central Nervous System (CNS) lesions, with superior sensitivity compared to alternative modalities like CT, ultrasonography, conventional X-ray etc. It is routinely used for the noninvasive assessment of brain tumors [4, 5]. A tumor (also called a neoplasm or lesion) is abnormal tissue that grows by uncontrolled cell division. Brain tumors are named after the cell type from which they grow - may be primary (starting in the brain) or secondary (spreading to the brain from another area). There are over 120 different types of brain tumors and four different grades from which common brain tumors include different types of gliomas, of which the most common one and most aggressive is Glioblastoma Multiforme (GBM) (which will be discussed later).

The primary use of MRI based medical image analysis for brain tumor studies is in diagnosis, patient monitoring and treatment planning, but it could also be useful in clinical trials. Moreover, developments in physiologic MRI including perfusion-weighted imaging (PWI), diffusion-weighted imaging (DWI), and metabolic imaging have led to a number of different markers that may lend insight into tumor physiology [20]. The integration of these parameters and then into analyses for patients particularly those diagnosed with GBM holds significant promise for improving clinical outcomes. In order for these parameters to be translated to the *holistic* (which is characterized by the belief that the parts of something are intimately interconnected and explicable only by reference to the whole or relating to or concerned with complete systems rather than with individual parts) multiforme there are many technical and biological challenges that need to be addressed. MRI also appears as an imaging modality that can follow, non-invasively, several micro-vascular and cellular parameters with a strong potential for the evaluation of new drugs on brain tumors [18].

## 1.2. Statement of the problem

Accompanied by a rush of new development of high technology and use of various imaging modalities, more challenges arise; for example, how to process and analyze a significant volume of images so that high quality information can be produced for disease diagnoses and treatment [5].

MRI is mostly used in diagnosis and treatment planning of cancers since it provides good soft tissue contrast and enables a better lesion detection and staging. The current MR imaging technology allows acquisition of multiple parameters for use in a more informed image analysis. In this regard, different relaxation and functional MR imaging techniques exist [7].

Relaxation based as well as functional MRI techniques reveal detailed anatomical and physiological information of interest. Examples include T1 and T2 relaxivity, intravascular contrast enhancement physiology and water diffusion [53]. Even though each of these conventional metrics has its own specific merits, there always exists a relationship between these different parameters which is usually less exploited despite the fact that such information is potentially very useful for image processing [6]. Besides it is usually the case that no single modality is capable of providing a comprehensive characterization of the object of interest (brain tissue in our case). To that end the idea of multi-parametric MR image (MP-MRI) analysis has recently gained a lot of attention. The very fundamental question is then how do we analyze the multiple parameters as one entity making use of the intrinsic inter-correlation information embedded among the different parameters. This is in particular as opposed to the traditional way of analysis that tries to first separate the different components and carry out the analysis serially [1, 2].

This thesis presents the development of a MP-MRI analysis technique that treats multiple MRI parameters as one entity for representation and discusses a holistic analysis technique based on a rigorous mathematical algorithm. The current study applies a novel color transformation scheme for use in processing MP-MRIs expressed as two dimensional multicomponent (color) signals in higher order algebraic spaces [1, 2].

Different data sets acquired at selected institutions in Ethiopia and overseas are used to test the proposed image processing scheme and also various statistical analysis are carried out on the results. The study also incorporates analysis comparing other scheme suggested in the literature for use in analyzing MP-MRIs including their computational efficiencies.

## 1.3. Objectives

### 1.3.1. General Objective

- To improve differentiation of neoplasms (abnormal growth of tissues) and normal brain tissues using the information provided by MP-MRI images to provide an automated tool that assist physicians in better imaging evaluation of brain cancer tumors.

### 1.3.2. Specific Objectives

1. To combine multiple MRI parameters like T1, T2, Proton Density (PD), and Apparent Diffusion Coefficient (ADC) as one color image represented in a suitable color space.
2. To analyze the combined MP-MRI holistically using higher order Fourier transforms using vectorial approach.
3. To prove the concept that MRIs carry much useful information compared to other imaging modalities such as CT due to its high soft tissue contrast and flexibility for structural, functional and metabolic measurements.
4. To investigate the potentials of the proposed image processing algorithm for extraction of useful biomarkers for use in brain cancer patients' response quantification (such as disease progression and survival).
5. To learn more about underlying physics of the images.

## 1.4. Significance of the study

The mounting occurrence of malignant brain tumors increases the number of medical images that need to be studied by physicians. Further, expensive cost of efficient and effective investigations for better treatment and the lack of experts inhibit numerous patients from getting the right medical care. The visual analysis traditionally used by physicians for studying tumors has at least known

shortcomings: it is time consuming, is hardly repetitive, suffers from observer variability issues and often times less accurate [2]. Consequently, algorithmic medical image analysis is an important biomedical application which is highly computational in nature and requires the development of automated systems to circumvent these and many other difficulties. In that regard this thesis discusses the development of a holistic image processing tool mainly for use in automatic identification of tumor voxels based on conventional parameters derived from MR imaging [1]. MR images taken from brain tumor patients before, during, and after treatment are used for sophisticated image processing task of robustly differentiating lesions and normal brain tissues with the intent to derive image based biomarkers that could be used in patients' treatment response quantification and monitoring [71].

## 1.5. Scope of the Thesis

This thesis intends to address the use of sophisticated image processing algorithm for use in cleverly analyzing MP-MR images towards effective and efficient detection of glioma (GBM) cancers with potential implications in treatment response quantification. The results presented might still need rigorous validation including an observer study. The clinical evaluation of the method is awaiting further research and such issues are beyond the scope of the current study.

## 1.6. Organization of the thesis

This thesis is comprised of seven chapters divided into different sections: chapter one provides background information about general imaging technology, statement of the thesis problem, its objectives and scopes. Chapter two summarizes gliomas and brief overview of radiation and its effects on humans, overview of MRI system hardware components and duties, physics and fundamental phenomenon. Chapter three discourses about medical imaging and some important imaging modalities like anatomical, functional, and related technologies like X ray, Ultrasonography, Computed Tomography (CT), MRI, Positron Emission Tomography (PET), Endoscopy and Stereoscopy, accompanied by their comparative benefits and drawbacks and the importance of hydrogen atom as our

MR imaging source and proton precession and Larmor frequency is also discussed. Chapter four confers about medical image processing and its steps, color image processing and different color models available–particularly the RGB, CMY and HSI models and their variants. Topics including image preprocessing, reconstruction, registration, and image segmentation, particularly to do with MR image analysis are conferred in the final part of the chapter. Chapter five presents automatic brain tumor detection based on holistic multi-parametric magnetic resonance images (MP-MRIs) and their analysis for different applications including tissue classification, segmentation and the like. It presents the basics of the principal component analysis (PCA) and its linear transformation, trinions, quaternions, and their respective higher order integral transforms. It presents the proposed holistic image processing design for use in robust tumor detection of MP-MR images. Chapter six presents result and discussion while chapter seven weighs up the conclusion and future directions.

# Chapter 2. Fundamental particles and Brain tumor, MRI Hardware physics and Fundamental Phenomenon

## 2.1 Classification of fundamental particles: overview

Two classes of fundamental particles are known: *quarks* and *leptons*.

*Quarks* are particles that exhibit strong interactions. They are constituents of hadrons (protons and neutrons) with a fractional electric charge ($^2/_3$ or $-^1/_3$) and are characterized by one of three types of strong charge called color: red, blue and green. There are six known quarks: up, down, strange, charm, top and bottom.

*Leptons* are particles that do not interact strongly. Electron, muon, tau and their corresponding neutrinos fall into this category [59, 60].

*Electrons*, emitted from nuclei by *β*− radioactive decay and referred to as *beta particles* [60] play an important role in medical physics. They are used directly as beams for cancer therapy, they are responsible for the dose deposition in media by photon and electron beams, and they govern the experimental and theoretical aspects of radiation dosimetry[1] [59].

### 2.1.1 Classification of Radiation

Radiation is classified into two main categories, nonionizing and ionizing, depending on its ability to ionize matter (Fig. 1.1) [59].

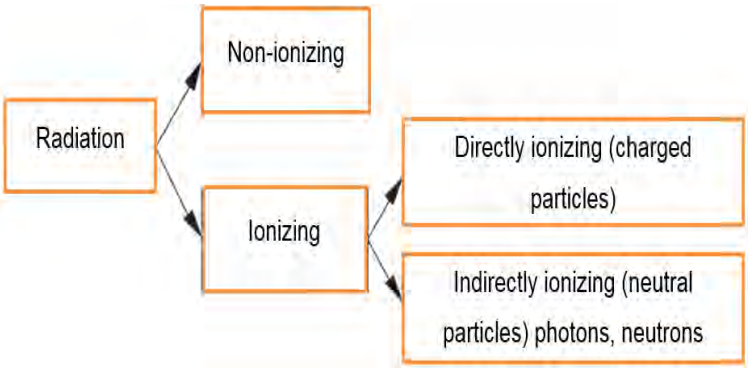


Figure 2.1: Classifications of Radiation [Curtsy of Introduction to Radiation Minister of Public Works and Government Services Canada. 2012]

[1]*Dosimetry, in its original sense is the measurement of the absorbed dose delivered by ionizing radiation better known in health physics and medical physics, where it is the calculation and assessment of the radiation dose received by the human body. It is used extensively for radiation protection and is routinely applied to occupational radiation workers, required treatment absorbed dose and any collateral absorbed doses where irradiation is expected, but regulatory levels must not be exceeded.*

The branch of medicine that uses radiation in the treatment of disease is called radiotherapy, therapeutic radiology or radiation oncology. Diagnostic radiology and nuclear medicine are branches of medicine that use ionizing radiation in the diagnosis of diseases. Non-ionizing radiation (cannot ionize matter) while ionizing radiation (can ionize matter either directly or indirectly) [59].

Directly ionizing radiation (charged particles): electrons, protons, α (alpha) particles and heavy ions whereas indirectly ionizing radiation (neutral particles): photons (X-rays and $\gamma$ rays), neutrons. Both directly and indirectly ionizing radiations are used in the treatment of diseases, mainly but not exclusively for malignant diseases [60].

Directly ionizing radiation deposits energy in the medium through direct Coulomb interactions between the directly ionizing charged particle and orbital electrons of atoms in the medium. Indirectly ionizing radiation (photons or neutrons) deposits energy in the medium through a two-step process. In the first step a charged particle is released in the medium (photons release electrons or positrons, neutrons release protons or heavier ions). In the second step the released charged particles deposit energy to the medium through direct Coulomb interactions with orbital electrons of the atoms in the medium [42].

Ionizing radiation can be either alpha or beta particles, or high energy electromagnetic waves with enough energy to completely remove an electron from an atom [60]. Ionizing radiation is used daily in hospitals and clinics to perform diagnostic imaging exams and medical interventions. For the purposes of this, the word radiation refers to ionizing radiation [61].

### 2.1.2 Classification of Ionizing Photon Radiation

*Characteristic X-rays*: resulting from electron transitions between atomic shells.

*Bremsstrahlung:* resulting from electron–nucleus Coulomb interactions.

**γ**-rays: resulting from nuclear transitions.

*Annihilation quanta:* resulting from positron–electron annihilation.

The most common forms of radiation in medicine are X-rays and gamma rays [42].

### 2.1.3 Radiation effects

In large doses, ionizing radiation can be hazardous and can cause burns to the skin and sickness. In medical imaging radiation doses are too low to cause serious damage, though there are still risks. Radiation can damage the DNA in cells. Sometime the cells can repair the damage, though sometimes they cannot and die. This fact is useful in the treatment of cancer where radiotherapy is used to kill the cells in a tumor. Another problem is that radiation can change the DNA without the cell dying. This is called mutation, and mutations can lead to the person being more likely to develop cancer later in life, or can be passed on to their children, sometimes leading to genetic abnormalities [61].

## 2.2 Brain tumors: Overview

A brain tumor is an intracranial mass produced by an uncontrolled growth of cells either normally found in the brain such as neurons, lymphatic tissue, glial cells, blood vessels, pituitary and pineal gland, skull, or spread from cancers primarily located in other organs. Generally speaking, brain tumors are classified based on the type of tissue involved, the location of the tumor, whether it is ***benign*** or ***malignant***, and other considerations. Primary (true) brain tumors are the tumors that originated in the brain and are named for the cell types from which they originated. They can be benign (non-cancerous), meaning that they do not spread elsewhere or invade surrounding tissues. They can also be malignant and invasive (spreading to neighboring area). Secondary or metastasis brain tumors take their origin from tumor cells which spread to the brain from another location in the body. Most often cancers that spread to the brain to cause secondary brain tumors originate in the lung, breast, and kidney or from melanomas in the skin [5].

Each primary brain tumor, in addition to the solid portion of the tumor, may have other associated parts such as edema and necrosis. Edema is one of the most important factors leading to mortality associated with brain tumors [16]. By definition, brain edema is an increase in brain volume resulting from increased sodium and water content and results from local disruption of the blood brain barrier (BBB). Edema appears around the tumor mainly in white matter regions [6]. Tumor associated edema is visible in MRI, as either hypo-intense (darker than

brain tissue) or rarely iso-intense (same intensity as brain tissue) in T1-weighted scans, or hyper-intense (brighter than brain tissue) in T2-weighted and FLAIR (Fluid-attenuated Inversion Recovery) MRI. Necrosis is composition of dead cells in the middle of the brain tumor and is seen hypo-intense in T1-weighted images. A brain tumor may also infiltrate the surrounding tissues or deform the surrounding structures. The different MRI parameters (T1, T2, …) are to be discussed in the next chapter.

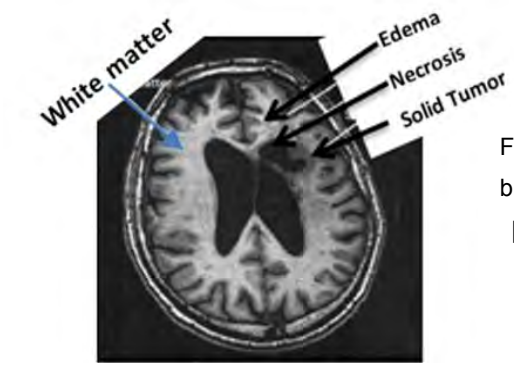


Figure 2.2: one axial slice of a MR image of the brain showing solid tumor, necrosis and edema [Curtsy of P. Reimer et al. (eds.), Clinical MR Imaging, Springer-Verlag Berlin Heidelberg 2010]

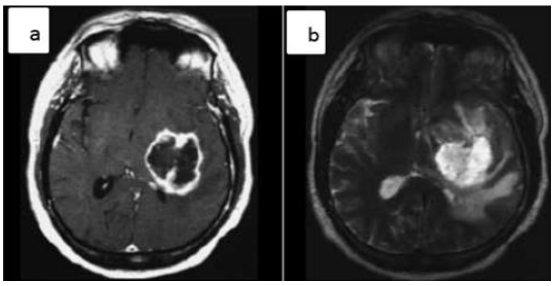


Figure 2.3: Glioblastoma Multiforme:

(a) Contrast enhanced axial T1-weighted of a ring enhanced tumor (necrotic)

(b) Axial T2-weighted image of the same tumor showing the surrounding edema [Curtsy of Biomedical Imaging and Intervention Journal: "A novel automatic method for extraction of glioma tumor, white matter and grey matter from brain magnetic resonance images" PP: 3]

## 2.3 Glioma tumors: Overview

Gliomas are the most frequent primary brain tumors that originate in glial cells. Glial cells are the building-block cells of the connective, or supportive tissue in the central nervous system (CNS) [1, 2]. According to the World Health Organization (WHO), gliomas are classified into four grades that reflect the degree of malignancy. Grades I and II are considered low-grade and grades III and IV are considered as high-grade. Grades I and II are the slowest-growing and least malignant, Grade III tumors are considered malignant and grow at a moderate rate. Grade IV tumors, such as Glioblastoma multiforme (GBM), are the fastest growing and the most malignant primary brain tumors [1, 3]. Being among the most

angiogenic human tumors, they are characterized by remarkable proliferative vascular components and are often necrotic and invasive [1]. Their aggressiveness is mainly due to their ability to stimulate the formation of new blood vessels [3]. Classification of glioma tumors is important for clinical understanding of tumor biology, clinical response and for assessing overall prognosis with brain tumors. However accurate grading of cerebral glioma using conventional structural imaging techniques remains challenging due to the relatively poor sensitivity and specificity of these methods [16].

## 2.4 MRI System Hardware and Physics: Overview

### 2.4.1 System Hardware

MRI scanners come in many varieties. We can have permanent, resistive, superconducting, and open or bore type magnets, with or without helium, low or high field strength. The choice of magnet is mainly governed by what we intend to do with it and how much money we have in the bank. High field magnets offer better image quality, faster scanning and a wider range of applications, but they are more expensive than their low field counterparts. The most important part in the system is the magnet. Fig. 2.4 presents a typical 1.5T, Siemens Avanto, state-of-the-art MRI machine.


Figure 2.4: Siemens Avanto 1.5T state-of-the art MRI machine [Curtsy of "Basics of MRI Professor" Sir Michael Brady FRS FREng Department of Engineering Science Oxford University Michaelmas 2004 PP.7.]

Within the bore of the magnet, there are the shim coils, gradient coils and RF coils. In the case of the 7T scanner, the RF coils are usually attached to the bed (see Fig. 2.5).

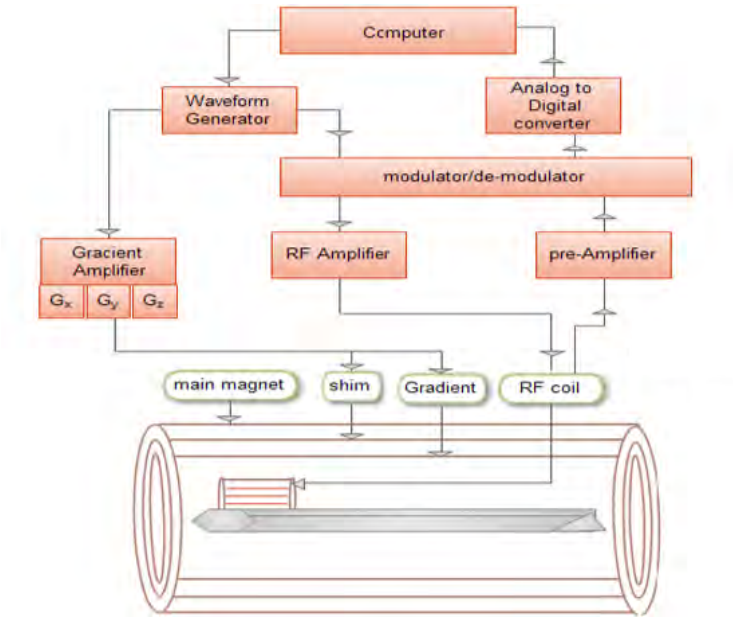


Figure 2.5: The MRI System [Curtsy of MRI Hardware: magnet, gradient, and RF coils Hsiao-Wen Chung, Ph.D., Professor Dept. Electrical Engineering, National Taiwan Univ. Dept. Radiology, Tri-Service General Hospital, 2011]

### 2.4.2 MRI Hardware components and duties

#### (A) The Main Magnet

Three magnet types are used in MR systems:

(A) Permanent Magnet

(B) Resistive Magnet and

(C) Superconducting Magnet

#### (A) Permanent Magnet

The permanent magnet systems are made of ferromagnetic material such as iron and are for field strengths up to 0.4T. The uniformity is achieved by a careful shaping of the pole faces. However, one major drawback is the heavy weight of these magnets; they can weigh up to 100 tons for whole body magnets. They have the virtue of producing low fringe field; have low maintenance costs and the open design is suitable for claustrophobic patients. However, they require temperature control to maintain the field uniformity.

#### (B) Resistive Magnets

Resistive magnets are rarely used nowadays. They consist of copper wires by which the magnetic field is generated. With such a magnet, a coolant system must be introduced due to the heat generated by the currents in the wires. For example,

a few millimeters in diameter of copper wire operating at room temperature carries about 100 amps continuously.

### (C) Superconducting Magnet

Today's most commonly used magnets are superconducting magnets. The magnetic field is generated by a current, which runs through a loop of wire. The wire is surrounded with a coolant, such as liquid helium, to reduce the electric resistance of the wire. At 4 Kelvin (-269$^{o}$C) electric wire loses its resistance. Once a system is energized, it will not lose its magnetic field. Superconductivity allows for systems with very high field strengths up to 12T. The ones that are most used in clinical environments run at 1.5T. Most superconducting magnets are bore type magnets. Figure 2.6 shows how a superconducting magnet is build up.

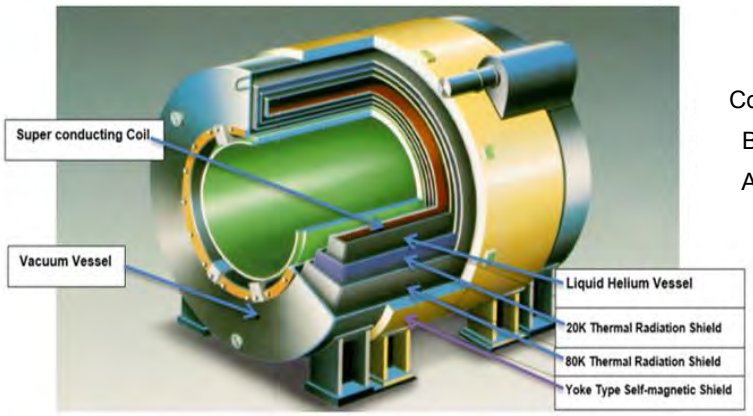


Figure 2.6: Section of Super-Conducting magnet MRI (Curtsy of Basic MRI physics; Evert J Blink Application Specialist MRI PP.7)

## 2.4.3 The Shim System

Shim coils are used to remove the inhomogeneity introduced during the magnet design process. It is almost impossible to construct magnets that are as homogeneous as specified by the theoretical designs. The inhomogeneity is caused by the difference in susceptibility between tissues, as well as structures around the magnet affecting the local magnetic field, leads to a requirement to have shim methods [30].

## 2.4.4 Gradient Coils

A gradient field superimposed on the static magnetic field results in a linear variation in magnetic field. This in turn causes the resonant frequency to vary as a function of position. Three orthogonal resistive coils are set inside the magnet bore to generate the additional linear variation of the field in all the three orthogonal

directions (x, y, z) [32]. Typically, they are capable of producing a linear variation over the volume of interest [26], (Fig. 2.7.)

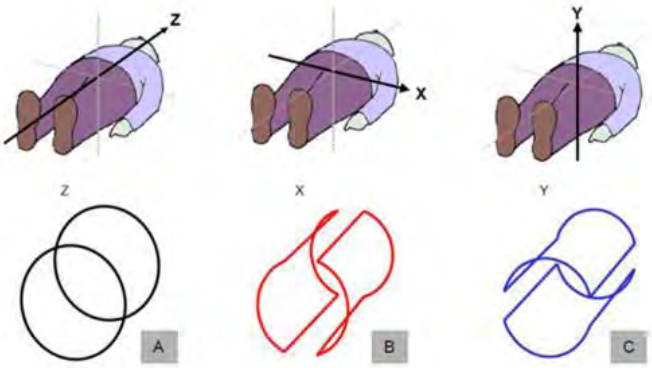


Figure 2.7: Gradient coils [Curtsy of Basic MRI physics; Evert J Blink Application Specialist MRI PP.7]

### 2.4.5 The RF System

RF coils need to generate a $B_1$ (a magnetic field generated by RF at the larmor frequency (the resonance frequency of protons) perpendicular to $B_0$) field orthogonal to the main field $B_0$ (strong homogenous static magnetic field) that is uniform over the imaged region. In an RF pulses, the $B_1$ field is used to flip the spins and hence generate a detectable NMR signal. In practice, to irradiate the tissues a transmitter associated with an RF coil is used while for detection a receiver associated with a separate RF coil is used [28]. Fig.2.8 shows the RF system block diagram.

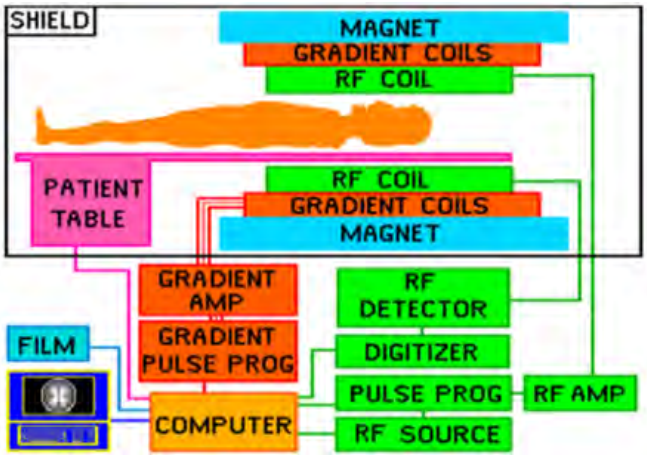


Figure 2.8: RF system block diagram [Curtsy of Overview of the Basic MR System Components Jerry Allison Ph.D., 2009]

## 2.5 MRI Basic Physics: Overview

MRI is the preferred imaging modality for the diagnosis of brain tumor diseases and for assessing response to therapy due to its high soft-tissue contrast. Contrast is based on the relative relaxation properties of hydrogen protons (spins) when

placed in a uniform magnetic field. At rest, these spins are randomly aligned, but in the presence of an external magnetic field ($B_0$) they align parallel or antiparallel to $B_0$. A slight excess of spins remains in the aligned, lower energy state resulting in a net magnetization vector, $M_o$ [9]. The distribution of spins in the higher (n-) and lower (n+) can be described as:

$$\frac{n^-}{n^+} = \exp\left(\frac{-\gamma B_o}{kT}\right) \qquad (2.1)$$

where k = Boltzmann's constant ($1.381 \times 10^{-23}$ $JK^{-1}$),

T = temperature in Kelvin (body $310.25^0$ K), and

$\gamma$= gyromagnetic ratio (42.58 MHz/T for $H^1$ proton).

An excitation radiofrequency pulse ($B_1$) can be delivered to the system perpendicularly to $B_0$ at the frequency f = ( $\frac{\gamma}{2\pi}$)$B_0$ to flip the parallel spins into the antiparallel, elevated energy level state.

The change in energy between these quantum states is defined by:

$$\Delta E = \frac{h\gamma}{2\pi} \qquad (2.2)$$

where h = Planck's Constant ($6.626 \times 10^{-34}$ $m^2kg/s$).

Using a classical description, this pulse can also be visualized as tipping the magnetization vector into the transverse plane (Fig. 2.10). The angle between the $B_0$ field and the magnetization vector M is called the flip angle and depends on the $B_1$ field and time it is applied:

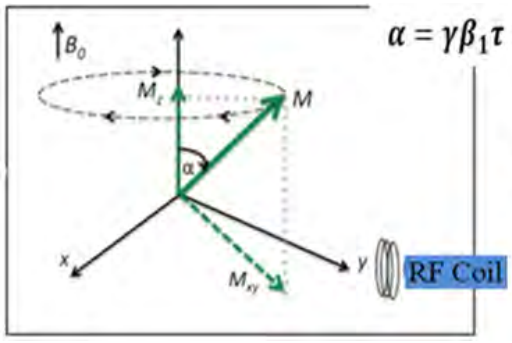


Figure 2.9: Diagram of M precession After Excitation, M is tipped away from the $B_0$ axis through angle α and precesses about $B_0$ with $M_{xy}(t)$ and $M_z(t)$ [Curtsy of Spinning Protons Presents: The Basics of MRI: T1 vs. T2, Frank Minja, , 2012]

After the $B_1$ pulse, the magnetization vector M precesses about the z-axis at the Larmor frequency, $\frac{\lambda}{2\pi}\beta_o$. There are two methods by which M returns to its initial $M_0$ state, which are described by two time constants: T1 and T2.

### 2.5.1 T1 and T2 Weighted Images

T1 or longitudinal relaxation time (Figure 2.11 (A)) represents the time required for a substance to regain its longitudinal magnetization (in the z- direction) following an RF pulse [11].

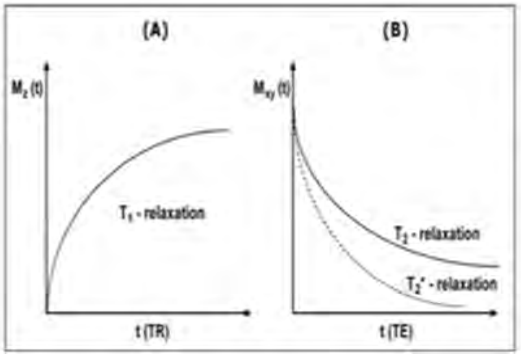


Figure 2.10: Diagram depicting exponential curves of (A) T1 and (B) T2, T2* relaxation [Curtsy of Physics of MRI, Yao Wang Polytechnic University, Brooklyn, NY, 2010]

T2 or transverse relaxation time (Figure 2.11(B)) is a measure of how long the resonating protons remain coherent or precess in phase following a RF pulse. Alternatively, it represents the loss of magnetization in the XY-plane [3]. There is also a dephasing effect caused by local field in-homogeneities, and its characteristic time is referred to as T2* relaxation (Fig. 2.11 (B)). T2* is always faster than the T2 decay. T1 and T2 relaxation are two independent processes, which happen simultaneously and T2 is much quicker than T1 [3].

### 2.5.2 Fluid Attenuated Inversion Recovery (FLAIR)

Fluid Attenuated Inversion Recovery (FLAIR) is an inversion-recovery pulse sequence used to nullify the signal from fluids. For example, it can be used in brain imaging to suppress cerebrospinal fluid (CSF) so as to bring out periventricular hyper-intense lesions, such as multiple sclerosis (MS) plaques.

## 2.6 MRI Fundamental Phenomenon: Overview

Spin is a fundamental property (like electrical charge or mass) of sub-atomic particles such as protons, electrons and neutrons. MRI produces images by exploiting the interaction between the nuclear spins and an externally applied strong homogenous static magnetic field, $B_0$. When the patient is placed in the magnet, the atomic nuclei or protons with a non-zero spin (e.g. hydrogen with a $\frac{1}{2}$spin) present in the body tends to align itself in the direction or against the

direction of $B_0$ almost cancelling each other out. However, a slightly bigger number of protons align in parallel with the applied magnetic field generating a net overall equilibrium magnetization, $M_0$ [20]. In this equilibrium state, only longitudinal magnetization ($M_z$) is present with no transverse magnetization ($M_x$ or $M_y$). At this stage RF pulses, exactly at the Larmor frequency (the resonance frequency of protons) are applied to generate a magnetic field $B_1$ perpendicular to $B_0$ field [62]. This causes the spins to excite causing them flip away from the z-axis and gain x- and y components while precessing (rotating) about the z-axis (see Fig. 2.10).

At the end of the applied RF pulse, the magnetization field $B_1$ returns to equilibrium from the excited state through interactions with the surrounding environment by a process called relaxation. The relaxation process follows an exponential curve and can be described by two time constants, $T_1$ and $T_2$. From a clinical perspective, they are useful because different tissues appear differently in $T_1$ and $T_2$ weighted MR scans. For example, $T_1$ images cause fat to appear bright, fat like the myelin in white matter whereas $T_2$ weighted images cause water to appear bright like CSF and fat is dark [11].

# Chapter 3. Medical Imaging and Important Imaging Technologies

As technology expands and cost-benefit questions intrude, recognition of the advantages and disadvantages of various imaging modalities is paramount in guiding patient management [17]. Medical imaging was primarily seen as the use of non-invasive techniques to create internal images of the human body for clinical or medical purposes (i.e. “virtual dissecting” of the human body). It has changed tremendously over the past decade, beginning with the basics, following with the breakthroughs, and moving on to the abstract [48].

Continuous innovations have been fueled by the need to improve diagnostic yield and achieve fast turnaround through robust information management, which should ultimately improve patient outcome. The rapid changes in digital technology have also created opportunities for the development of high-tech equipment employed in medical imaging practice [48]. Many different imaging techniques have been developed and are in clinical use. Because they are based on different physical principles, these techniques can be more or less suited to a particular organ or pathology. In practice they are complementary in that they offer different insights into the same underlying reality. In medical image processing, these different imaging techniques are called modalities [49].

*Anatomical modalities* provide insight into the anatomical morphology. They include radiography, ultrasonography or ultrasound, computed tomography (CT), magnetic resonance imagery (MRI). There are several derived modalities that sometimes appear under a different name, such as magnetic resonance angiography (MRA, from MRI), digital subtraction angiography (DSA, from X-rays), computed tomography angiography (CTA, from CT) etc. [48].

*Functional modalities*, on the other hand, depict the metabolism of the underlying tissues or organs. They include the three nuclear medicine modalities, namely, Scintigraphy (*a technique in which scintillation counter is used with a radioactive tracer to obtain an image of a bodily organ*), single photon emission computed tomography (SPECT) and positron emission tomography (PET) as well as

functional magnetic resonance imagery (fMRI). This list is not exhaustive, as new techniques are being added every few years as well [49]. Almost all images are now acquired digitally and integrated in a computerized picture archiving and communication system (PACS) [49].

## 3.1. Diagnostic Imaging: Overview

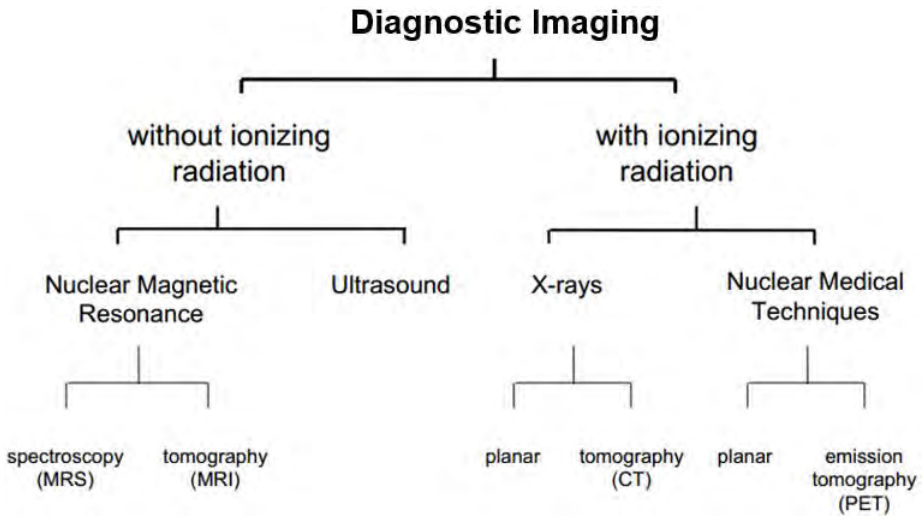


## 3.2. Some Important Imaging Technologies: Overview

All imaging techniques have one feature in common: the basis is the interaction between energy and matter. Tomographic imaging principles are rooted in physics, mathematics, computer science, and engineering [28]. During the past few decades, with the increasing availability of relatively inexpensive computational resources CT, MRI, Doppler ultrasound, and various imaging techniques based on nuclear emission (PET, SPECT… etc.) have all been valuable additions to the radiologist's arsenal of imaging tools toward ever more reliable detection and diagnosis of diseases [48].

### A. X-ray Radiography

Developed the first time in 1890s, X-ray radiography is one of the most commonly used methods of diagnosis. It can be used to examine broken or fractured bones, teeth, the digestive system, and the lungs and to detect breast cancer [48].

X-rays are produced when electrons hit a metal, which in hospital x-ray tubes, is usually tungsten. The x-rays then pass through the body and onto either a film cassette or digital detector (like in a digital camera). Structures in the body like

bones are very dense and contain elements such as calcium that have a high atomic number. This makes bone absorb a high proportion of the x-rays. Soft tissues like fat and muscle allow more x-rays to pass through [29]. The body casts an x-ray shadow onto the film. Where the x-rays have passed through bone, the film is less exposed so it looks white; where they have not passed through anything the film is exposed and turns black; and where the x-rays have passed through soft tissues of the film has different levels of grey [49].

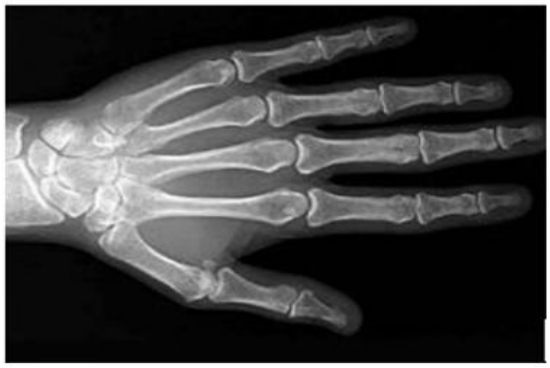

Figure 3.1: Skeleton of hand X-ray image [Curtsy of Vicente Gilsanz, Ph.D. Department of Radiology Children's Hospital Los Angeles Sunset Blvd., 2008]

## B. Ultrasonography

This was first introduced in 1960s. In this modality, a transmitter sends high frequency sound waves into the body where they bounce off the different tissues and organs to produce distinctive patterns of echoes. These echoes are acquired by a receiver and forwarded to a computer that translates them into an image on a screen. Because ultrasound can distinguish subtle variations among soft, fluid-filled tissues, it is particularly useful in imaging the abdomen [52].

Figure 3.2: Ultrasound imaging: development of pregnancy [Curtsy of Ultrasound in Obstetrics and Gynecology for the Generalist, Dr. S.Moola Ob/gyn - Nelson BC, 2012]

In contrast to X-rays, ultrasound does not damage tissues with ionizing radiation. The major disadvantage of ultrasonography is that it produces very noisy images. It may therefore be hard to distinguish smaller features (such as cysts in breast imagery). Typically, quite a bit of image preprocessing is required [49].

### C. Computed Tomography (CT)

CT was introduced in 1970s. CT scan (sometimes called computed axial tomography, or a CAT scan) is acquisition of sectional (tomographic) images by a number of 2D radiographs by use of an X-ray tube and detector rotating around the patient in a doughnut-shaped machine taking x-ray images of the slice from all angles around the body (there are several different geometries for this). The full 3D image can then be reconstructed by computer from the 2D projections using the *Radon transform* to produce a cross sectional image (a picture of a slice through the body). Thus CT is essentially a 3D version of X-ray radiography, and therefore offers high contrast between bone and soft tissue and low contrast among different soft tissues [49].

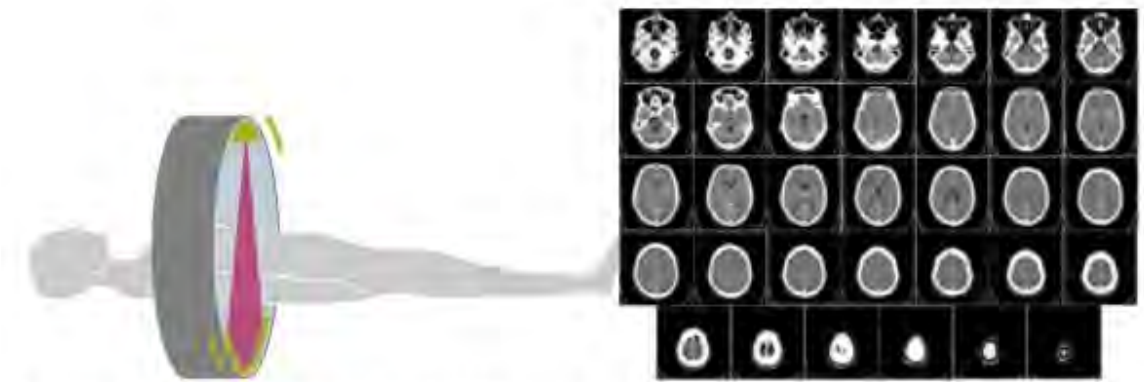

Figure 3.3: Computed tomography of human brain, from base of the skull top. Taken with intravenous contrast medium [Curtsy of CT Head Anatomy and Pathology, Jeanette Dadds BHH Louise Bishop GHH Shirley Atkinson SHH CT Clinical Co-ordinators, APRIL 2011]

CT is useful for diagnosing internal injuries in trauma victims. Because a scan takes only a couple of minutes it can find problems quickly and save their lives. One problem with CT and X-ray is the radiation dose to the patient. A scan of the abdomen gives a dose of 10mSv, which is equivalent to the natural background

radiation exposure over 4 years. This is about 100 times more than a standard chest X-ray [48].

### D. Endoscopy

Endoscopy means looking inside and typically refers to looking inside the body for medical reasons [50]. Unlike most other medical imaging devices, endoscopes are inserted directly into the organ. This advancement is represented by the incorporation of Charge-Coupled Device (CCD) (that converts optical image to electronic image) into gastrointestinal endoscopy [48,49]. These video endoscopes use Xenon arc lamps as light source. Two cameras are mounted on a single laparoscope. Images from the cameras are transmitted alternately to a video monitor. As the camera transmits images at 60-120 cycles per second a three-dimensional real time image is perceived. As the images are transmitted at a high frequency, the effect is that of seeing different images simultaneously [51].

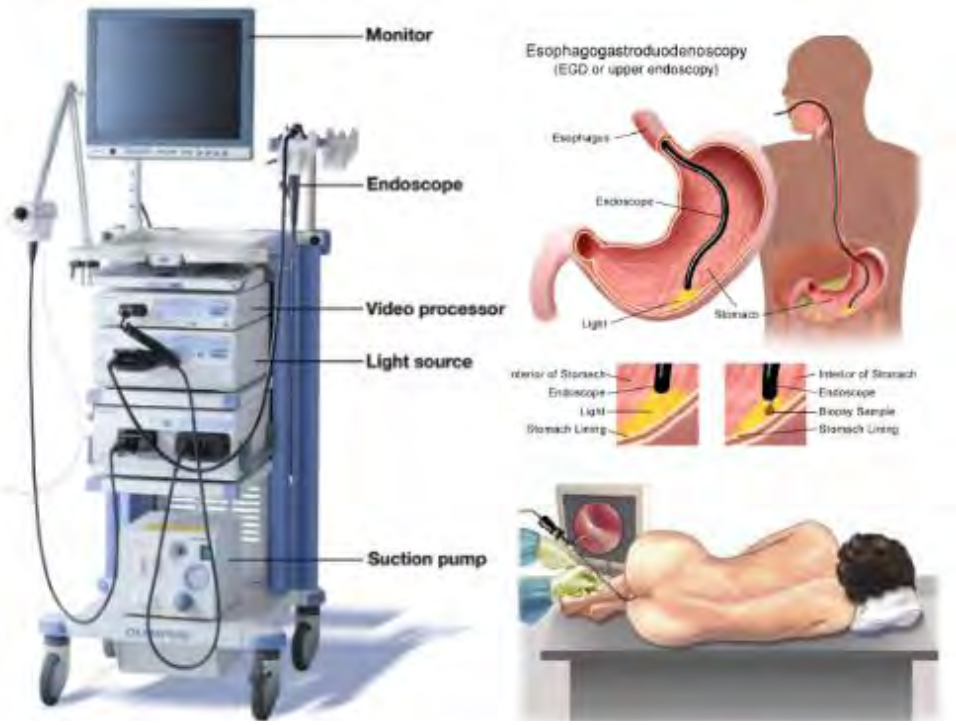


Figure 3.4: Example of a complete modem Endoscope system [Curtsy of Karl Storz Endoskope GmbH & Co. KG Industrial Group, MittelstraBe, Tuttlingen/Germany, 2013]

Color imaging is achieved by incorporating RGB filters between Xenon lamp supply and the proximal end of the endoscope. The other approach to the generation of color image is to divide the available cells on the CCD among the

three primary colors by means of filters. Three images one for each color are then produced simultaneously by the CCD. Endoscopic pictures are converted to digital images by using CCD cameras and associated image digitizer circuits into a PC/AT. The recorded images can be image processed for better quality [50].

### E. Laparoscopy

Laparoscopy (from Ancient Greek *λαπάρα* (lapara), meaning "flank, side", and *σκοπέω* (skopeo), meaning "to see") [51] is an operation performed in the abdomen or pelvis through small incisions (usually 0.5–1.5 cm) with the aid of a camera. It can either be used to inspect and diagnose a condition or to perform surgery.

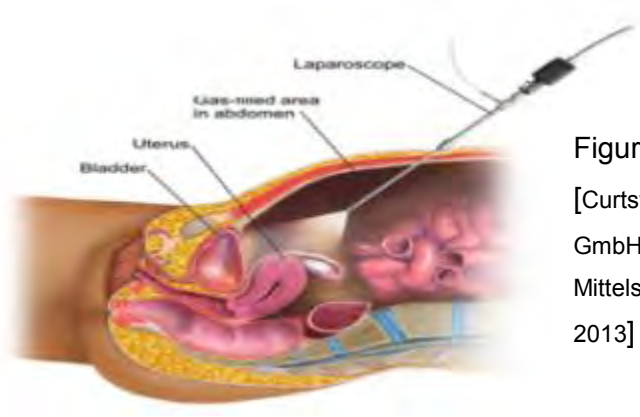


Figure 3.5: Laparoscopy [Curtsy of Karl Storz Endoskope GmbH & Co. KG Industrial Group, MittelstraBe, Tuttlingen/Germany, 2013]

### F. Magnetic Resonance Imaging (MRI)

First introduced in 1980s, as thoroughly discussed in the previous chapter, this technique relies on the relaxation properties of magnetically-excited hydrogen nuclei of water molecules in the body. The patient under study is briefly exposed to a burst of radio-frequency energy, which, in the presence of a magnetic field, puts the nuclei in an elevated energy state [49].

MRI distinguishes itself from other modalities and it can be applied in the volumetric analysis of muscles, heart and cancer, brain tissues such as multiple sclerosis, schizophrenia, epilepsy, cerebral atrophy etc. [62]. It does not use radiation, and its magnetic fields are thought to be safe. However, MRI scanners are very big and expensive. Also, because of the strong magnetic fields, all metal objects have to be kept out of the room or they would get pulled into the scanner.

People with pacemakers or other implanted devices cannot have MRI scans as the magnetic field would stop them working. An MRI scan can take up to 20-45 minutes to complete and you have to be still the whole time as any movement would blur the image. The changing magnetic fields also produce a lot of noise, which can be scary, and as you are inside the scanner during the scan, people with claustrophobia in particular can find the process upsetting.

The spatial resolution of X-ray images, when using special X-ray film, is excellent. This is particularly useful when looking at bone structures. The spatial resolution of MRI compared to that of X-ray is poor. In general one can use X-ray and CT to visualize bone structures whereas MRI is extremely useful for detecting soft tissue lesions.

## G. Positron Emission Tomography (PET)

PET was invented in 1990s. The patient is injected with radioactive isotopes that emit particles called positrons (anti-electrons). When a positron meets an electron, the collision produces a pair of gamma ray photons having the same energy but moving in opposite directions.

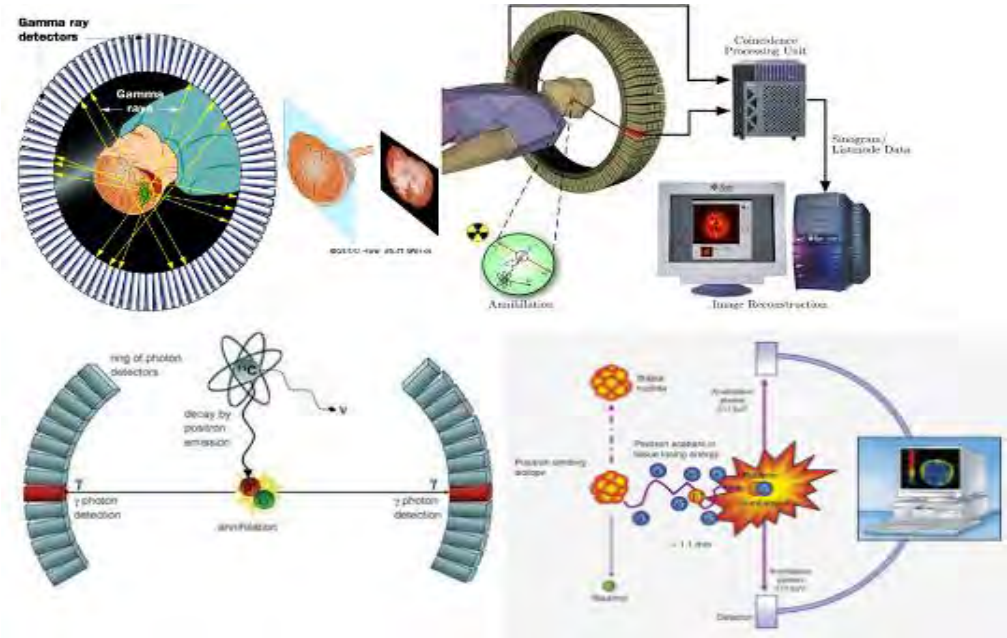


Figure 3.6: Positron emission tomography physics [Curtesy of Bailey, D.L; D.W. Townsend; P.E. Valk; M.N. Maisey, Positron Emission Tomography: Basic Sciences. Secaucus, NJ: Springer-Verlag, 2006]

From the position and delay between the photon pair on a receptor, the origin of the photons can be determined. While MRI and CT can only detect anatomical changes, PET is a functional modality that can be used to visualize pathologies at the much finer molecular level. This is achieved by employing radioisotopes that have different rates of intake for different tissues. For example, the change of regional blood flow in various anatomical structures (as a measure of the injected positron emitter) can be visualized and relatively quantified. Since the patient has to be injected with radioactive material, PET is relatively invasive. The radiation dose however is similar to a CT scan. Image resolution may be poor and major preprocessing may be necessary.

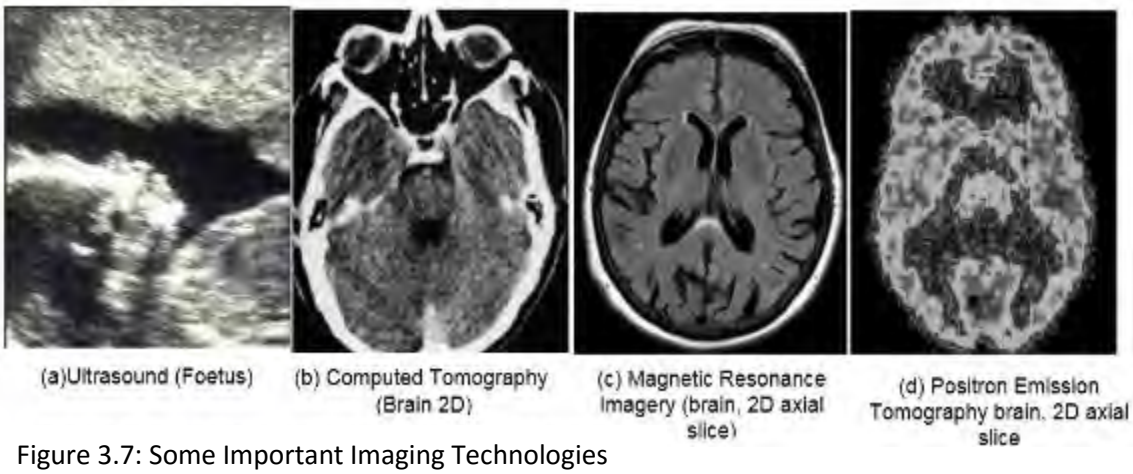


Figure 3.7: Some Important Imaging Technologies
[Curtsy of Brain Imaging Technologies and Their Applications in Neuroscience; By Carolyn Asbury, Ph.D.,]

Here, we mainly focus on the conceptual and functional overview of the principles of MRI, one of the major imaging modalities currently in use.

## 3.3. Principles of Magnetic Resonance Imaging Revisited

MRI is a tomographic imaging technique that produces images of internal physical and chemical characteristics of an object from externally measured nuclear magnetic resonance (NMR) signals [48].

An MR scanner shown in Fig. 3.8 consists of three main hardware components: *a main magnet*, *a magnetic field gradient system* and *a radio-frequency (RF) system*. The main magnet is a permanent magnet. It generates a strong uniform static field,

referred to as the $B_0$ field, for polarization of nuclear spins in an object. Most imaging systems operate at fixed field strength in units of Tesla [12]. The magnetic field gradient system normally consists of three orthogonal gradient coils, Gx, Gy and Gz, essential for signal localization. The gradient field strength is usually less than 1 Gauss per centimeter (G/cm). The RF system consists of a transmitter coil that is capable of generating a rotating magnetic field, referred to as the $B_1$ field, for exciting a spin system, and a receiver coil that converts a precessing magnetization into an electrical signal. On human imaging systems, the strength of $B_1$ is typically a small fraction of a Gauss [48].

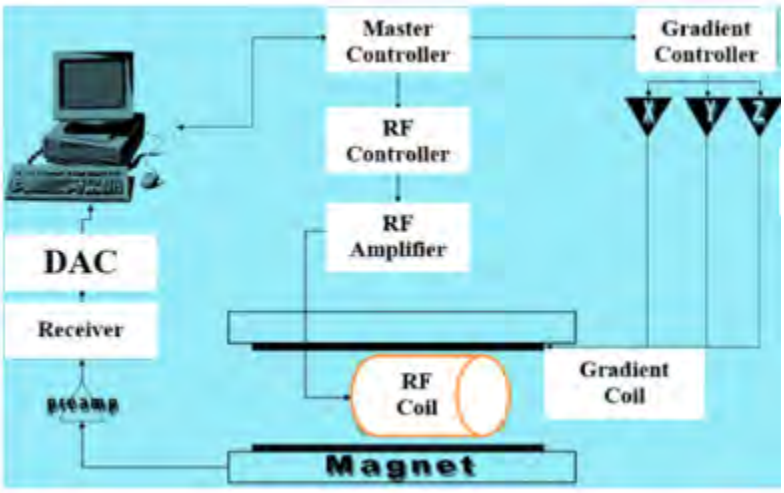


Figure 3.8: Simplified drawing of the basic instrumentation [Curtsy of Medical Image Processing Overview Hongmei Zhu, University of Calgary PP.2, 2011]

The orientation of the image is controlled by varying the main magnetic field using gradient coils. As these coils are rapidly switched on and off they create the characteristic repetitive noises of an MRI scan. The contrast between different tissues is determined by the rate at which excited atoms return to the equilibrium state. Exogenous contrast agents may be given intravenously, orally or intra-articularly (inter joint) [7], since in certain cases, the intrinsic differences in T1, T2, PD, etc., may not be sufficient to achieve the desired degree or kind of contrast, additional differences can be introduced by adding contrast agents. They are paramagnetic chemicals that localize in certain tissues/fluids, and artificially change their magnetic spin relaxation properties.

MR signals used for image formation come directly from the object itself. To understand how MR signals are generated requires understanding of quantum mechanics in the classical vector model [10].

Atoms with an odd number of protons and/or an odd number of neutrons possess a nuclear spin angular momentum, and therefore exhibit the MR phenomenon. Qualitatively, these nucleons can be visualized as spinning charged spheres that give rise to a small magnetic moment shown in Fig. 3.9 referred to as spins [48].


Figure 3.9: Nuclei with a nonzero spin are regarded as Microscopic Magnets [Curtsy of Medical Image Processing Overview Hongmei Zhu, University of Calgary PP.3]

In the absence of an external magnetic field, the spins are oriented randomly due to thermal random motion and the net macroscopic magnetic moment is zero as shown below (Fig 3.10a). To activate macroscopic magnetism from an object, it is necessary to line up the spin vector. This is accomplished by exposing the object to a strong external magnetic field $B_0$. The magnetic moment vectors tend to align in the direction of $B_0$ (referred to as the Z direction) to create a net magnetic moment M (Fig. 3.10b).

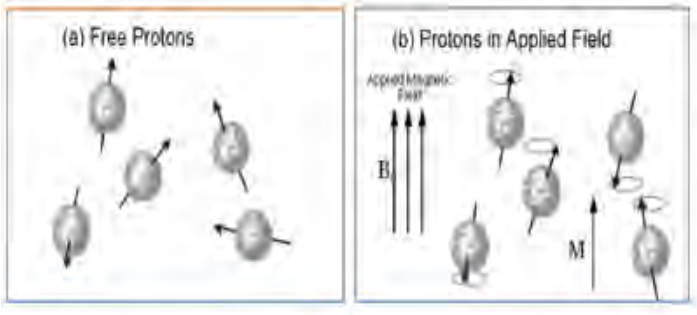


Figure 3.10: Nuclear Magnetic Moment Vectors:
(a) Pointing in random direction and
(b) Aligned in the direction of an external magnetic field
[Curtsy of Medical Image Processing Overview Hongmei Zhu, University of Calgary PP.4]

Also, the spins exhibit resonance at a well-defined frequency, called the Larmor frequency $\omega$. The Larmor frequency is defined as:

$$\omega = \gamma \beta o \qquad (3.1)$$

or

$$f = \frac{\gamma}{2\pi} \beta o \qquad (3.2)$$

where $\gamma$, the gyromagnetic ratio, is a known constant for each type of atom.

For $^1$H,

$\frac{\gamma}{2\pi}$= 42.58 MHz/Tesla. (3.3)

As an analogy, precession of a nuclear spin about an external magnetic field is similar to what a spinning top does in a gravitational field, (see Fig. 3.11).

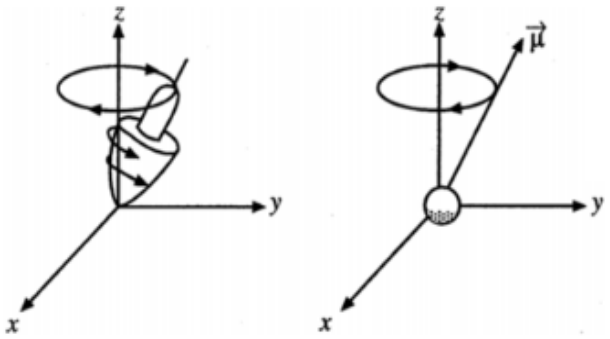


Figure 3.11: Precession of a Nuclear Spine about an external magnetic field is similar to the wobbling of a spinning top in a gravitational field.

[Curtsy of Medical Image Processing Overview Hongmei Zhu, University of Calgary PP.4)

## 3.4. Why do we take hydrogen as our MR imaging source?

There are two reasons. First of all we have a lot of them in our body. Actually it's the most abundant element we have (our body consist of about 80% water). Secondly, in quantum physics there is a thing called "Gyro Magnetic Ratio". Suffice to know that this ratio is different for each proton. It just so happens that this gyromagnetic ratio for Hydrogen is the largest; 42.58 MHz/Tesla [32]. When we put a person in a magnet some interesting things happen to the hydrogen protons:

1. They align with the magnetic field. This is done in two ways, parallel or anti-parallel. ($B_0$ is the indication for the magnetic field of the MRI scanner).
2. They precess at the Larmor frequency or "wobble" due to the magnetic momentum of the atom [32].

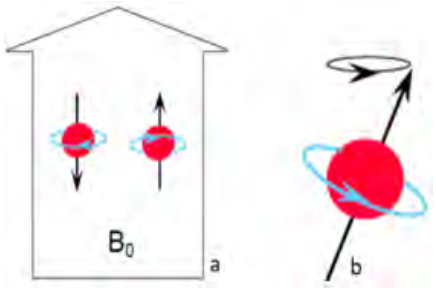


Figure 3.12:
(a) Hydrogen protons align with magnetic field
(b) Hydrogen proton precess at the Larmor frequency due to the magnetic momentum of the atom [Curtsy of Basic MRI physics; Evert J Blink Application Specialist MRI PP.12]

Hydrogen is not the only element we can use for MR imaging. In fact any element, which has an odd number of particles in the nucleus, can be used. Some elements, which can be used, are shown in Table 3.1 [28].

Table 3.1: MRI friendly elements [Curtsy of Basic MRI physics; Evert J Blink, MRI PP.12]

| Isotopes | Symbol | Spin Quantum Number | Gyro Magnetic Ratio(MHz/T) |
|---|---|---|---|
| Hydrogen | $^{1}H$ | ½ | 42.6 |
| Carbon | $^{13}C$ | ½ | 10.7 |
| Oxygen | $^{17}O$ | $^{5}/_{2}$ | 5.8 |
| Fluorine | $^{19}F$ | ½ | 40.0 |
| Sodium | $^{23}Na$ | $^{3}/_{2}$ | 11.3 |
| Magnesium | $^{25}Mg$ | $^{5}/_{2}$ | 2.6 |
| Phosphorus | $^{31}P$ | ½ | 17.2 |
| Sulphur | $^{33}S$ | $^{3}/_{2}$ | 3.3 |
| Iron | $^{57}Fe$ | ½ | 1.4 |

Therefore, in biological specimens, hydrogen ($^{1}H$), with a single proton, is the most abundant (the body consists largely of $H_2O$), the most sensitive and by far the most studied. Therefore, we usually refer to $^{1}H$ (proton) imaging [48]. The Larmor (precession) $(\omega)$ frequency (Larmor equation) can be calculated from the following equation.

$$\omega_0 = \gamma \beta_0 \qquad (3.4)$$

$\omega_0$= Precessional or Larmor frequency (MHz)

$\beta_0$= Magnetic Field Strength (T)

$\gamma$=Gyromagnetic Ratio (MHz/T)

Here we see two things, the Gyro Magnetic Ratio and the Magnetic field strength. $\omega_0 = \gamma B_0$, for water protons in 1 Tesla field, Larmor precession frequency is $\approx 42.58$ MHz (Resonance Frequency). This means if an external RF signal of Larmor frequency or Resonance frequency (i.e. 42.58 MHz in 1 Tesla MRI unit) is applied, water protons can absorb energy from external RF signal [28].

Once protons influenced by external RF signal, two effects are observed:

1) Protons become synchronized with external RF signal (and hence start precessing in-synchrony with each other).
2) Protons absorb energy from external RF signal (of resonance frequency) by tipping their spin axis by 180 degrees- they "tip upside down" [36].

At equilibrium, the transverse component of $M_0$ (i.e., the projection of $M_0$ in the X-Y plane, namely, $M_{xy}$) is zero (Fig 3.13a). To obtain MR signal, a RF field $B_1$ applies an external force along the transverse plane to excite these spins out of equilibrium and tip $M_0$ away from the z-axis (the direction of $B_0$), creating a measurable (nonzero) transverse component $M_{xy}$ (Fig. 3.13b). When turning the excitation off, relaxation back to its equilibrium also occurs with the length of the magnetization vector not remaining constant over time.

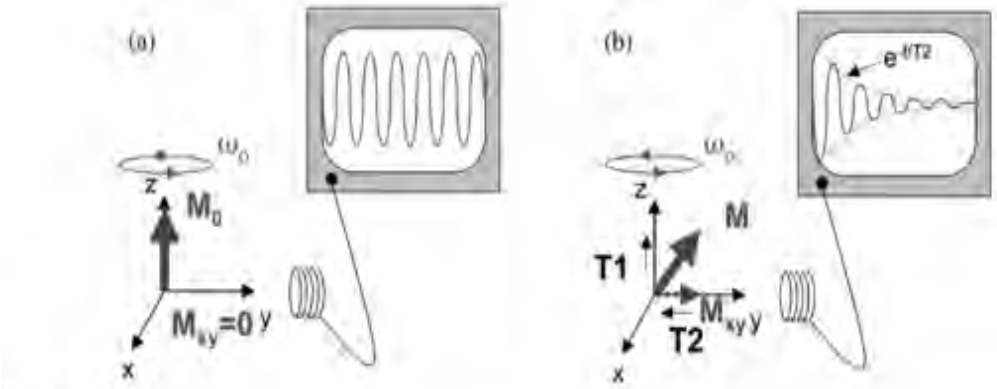


Figure 3.13:

(a) The processing nuclie induce a voltage in a receiver coil placed parallel to the x-y plane. Frequency of induced voltage is the same as the precessional frequency $\omega_0$.

(b) Detected signal is modulated by the fundamental relaxation process, T1 and T2 decays. Both processes decrease as $M_{xy} \longrightarrow M_0$

**[Curtsy of Medical Image Processing Overview Hongmei Zhu, University of Calgary PP.5]**

The time constant characterizing the return of the magnetization vector along the z-axis (longitudinal axis) is called T1, while the time constant characterizing the decay of the transverse component is called T2. In humans, T1 values of most tissues range from about 100-1500 ms (Fig. 3.14), and its values increase as $B_0$ increases. T2 values range from about 20-300ms (Table 3.2) and it is largely independent of field strength.

Table 3.2: T2 of some normal tissue types [Curtsy of https://www.imaios.com/en/e-Courses/e-MRI/MRI-signal-contrast/Signal-weighting]

| Tissue | T2(ms) |
|---|---|
| Gray matter | 100 |
| White matter | 92 |
| Muscle | 47 |
| Fat | 85 |
| Kidney | 58 |
| Liver | 43 |

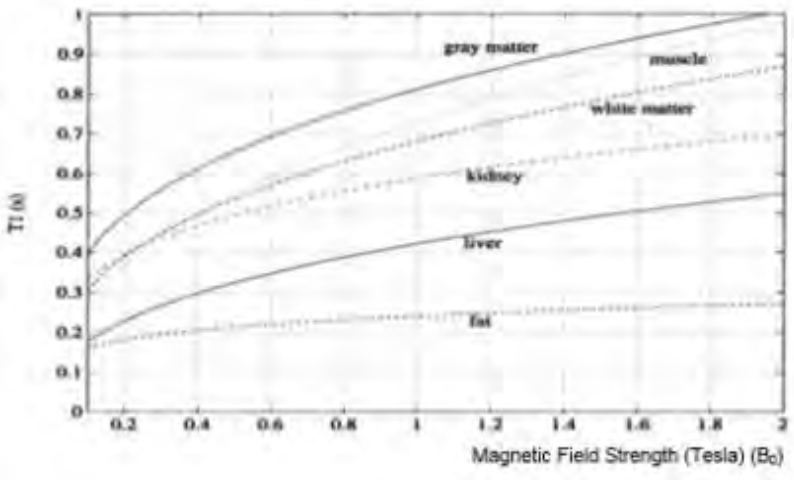


Figure 3.14: Approximate T1 value as a function of $B_0$ [Curtsy of Medical Image Processing Overview Hongmei Zhu, University of Calgary PP.5]

MR images are extremely rich in information content. The image pixel value can be considered as a function of a host of parameters, including the relaxation time constants T1 and T2, proton density (that has distinct values for different tissues), and the others.

Therefore, by changing the effect of these parameters, MR images obtained from the same anatomical position can look drastically different (see Fig. 3.15). These images can be further processed to produce new maps regarding water diffusion, blood flow, etc. Hence, the flexibility in data acquisition and the rich contrast

mechanisms of MRI endow the technique with superior scientific and diagnostic values as shown below [48].


Figure 3.15: Three images (a) T2-weighted (T2w), (b) T1-weighted (T1w), and (c) proton density (PD) images obtained from the same cross section of a human head

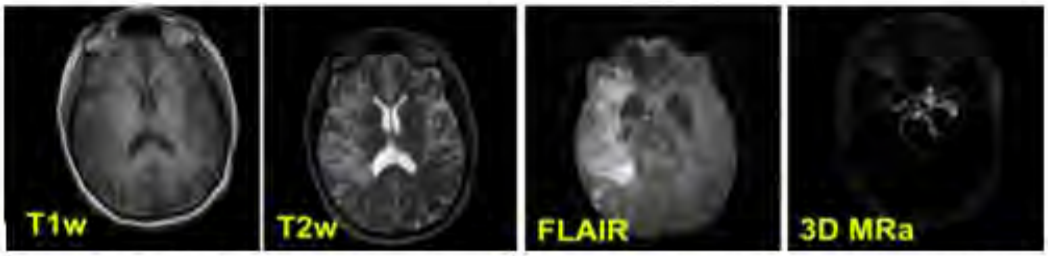


Figure 3.16: Multiple MR images were acquired to help neurologists diagnose a stoke patient who had middle cerebral artery occlusion in comparison to the right side of the brain [Curtsy of Medical Image Processing Overview Hongmei Zhu, University of Calgary PP.77]

## 3.5. MR imaging (or "pulse'') sequences

MRI imaging (or "pulse") sequences are a preselected set of defined RF and gradient pulses, usually repeated many times during a scan, wherein the time interval between pulses and the amplitude and shape of the gradient waveforms will control NMR signal reception and affect the characteristics of the MR images. In other words, an MRI pulse sequence is a programmed set of changing magnetic gradients. Different pulse sequences allow the radiologist to image the same tissue in various ways, and combinations of sequences reveal important diagnostic information about the tissue in question. Pulse sequences are computer programs that control all hardware aspects of the MRI measurement process. They are in essence a way to obtain information about the T1 and T2 characteristics of the target to be imaged.

Pulse sequences are used to generate the information from which MRI images are computed and ultimately generated. The most common sequences used in MRI

are the spin echo and gradient echo sequences. The RF signal received during an imaging sequence form a collection of time-varying multi-frequency RF signals (the "RAW" data matrix, or K-space matrix). These signals are manipulated by Fourier transformation to calculate the final images (i.e. MRI "pictures").

### 3.5.1. The Spin Echo (SE) sequence

The most common pulse sequence used in MR imaging is based on the detection of a spin "echo". It uses 90° radio frequency pulses to excite the magnetization and one or more 180° pulses to refocus the spins to generate signal echoes named spin echoes (SE). In the pulse sequence timing diagram show in Fig. 3.17, the simplest form of a spin echo sequence is illustrated.

The 90° excitation pulse rotates the longitudinal magnetization ($M_z$) into the xy-plane and the de-phasing of the transverse magnetization ($M_{xy}$) starts. The following application of a 180° refocusing pulse (rotates the magnetization in the x-plane) generates signal echoes. The purpose of the 180° pulse is to re-phase the spins, causing them to regain coherence and thereby to recover transverse magnetization, producing a spin echo.

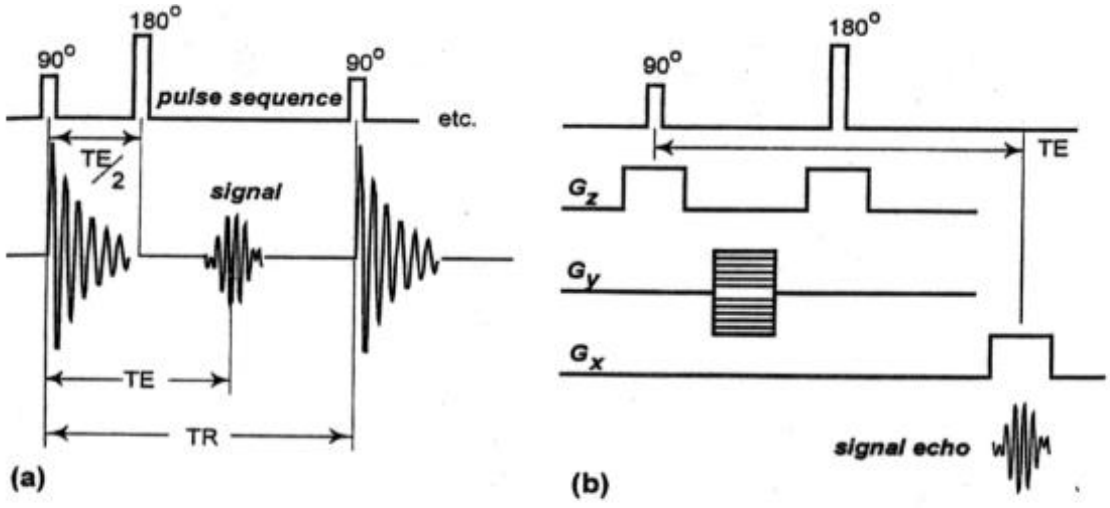


Figure 3.17: (a) The basic spin-echo pulse sequence identifying TR and TE together with τ which is TE/2
(b) The spin echo sequence with gradient switching Gz, Gy, Gx and echo signal timing which yields the 2D image

[Curtsy of Medical Image Processing Overview Hongmei Zhu, University of Calgary PP. 68]

Note that the figures on the left (a) depict the behavior of RF pulses while the right-hand figures (b) show the shape of the gradient fields, and both (a) and (b) occur at the same time.

- A 90$^o$ RF pulse at a predominant frequency is transmitted while $G_z$ is switched on.
- The center frequency of this pulse selects the position on the z-axis; its bandwidth determines slice thickness for a given gradient strength.
- Gy is now switched on changing the proton Larmor frequency. When the y-gradient is switched off the protons revert to their original Larmor frequency but they are de-phased so giving a phase difference. A single phase gradient is not sufficient to encode the entire y-axis so it is applied in carefully scaled steps.
- A rephrasing 180$^o$ signal after time TE/2 re-establishes phase relationships and the photons again have phase coherence.
- Just before TE time the $G_x$ is switched on which distributes the Larmor frequencies depending on proton position along the x-gradient.
- Echo signals are received and digitized (fast ADC) and stored in a voxel matrix according to their position determined by their phase and frequency in a k-space (frequency and phase matrix).

This total process is repeated a number of times with further 90$^o$ – 180$^o$ pulse sequences. The following points should be noted about the data stored as phase/frequency information.

- The central voxel represents zero frequency and zero-phase shift differences.
- The k-space matrix is converted to the conventional display matrix 256 X 256 or 512 X 512 which carries gray scale information depending on signal strength.
- A Fourier Transform converts the k-space into and x and y pixel matrix each carrying a gray scale value (e.g. for 8 bit image: 256 gray scales).

In the simplest form of SE imaging, the pulse sequence has to be repeated as many times as the image has lines. The SE pulse sequence exists now in many forms: the multi echo pulse sequence using single or multi-slice acquisition, the fast spin echo (FSE/TSE) pulse sequence, echo planar imaging (EPI) pulse

sequence and the gradient and spin echo (GRASE) pulse sequence; all are basically spin echo sequences.

Another representation of a standard Spin Echo sequence is shown in Fig. 3.18. In this type of representation, ADC refers to the time when the MRI units' receiver is ON and the signal is received and converted to a digital format (Analog to Digital conversion).

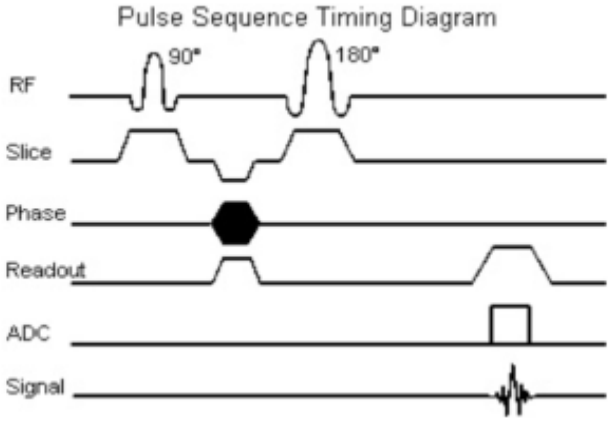


Figure 3.18: The basic spin-echo pulse sequence [Curtsy of J. E. Tanner & E. O. Stejskal "Spin-Echo Method"].

### 3.5.2. The Fast Spin Echo (FSE) sequences

The pulse sequence timing diagram shown in Fig. 3.19 illustrates a fast spin echo sequence with an echo train length of 3. This sequence is characterized by a series of rapidly applied 180$^{o}$ rephrasing pulses and multiple echoes, changing the phase encoding gradient for each echo.

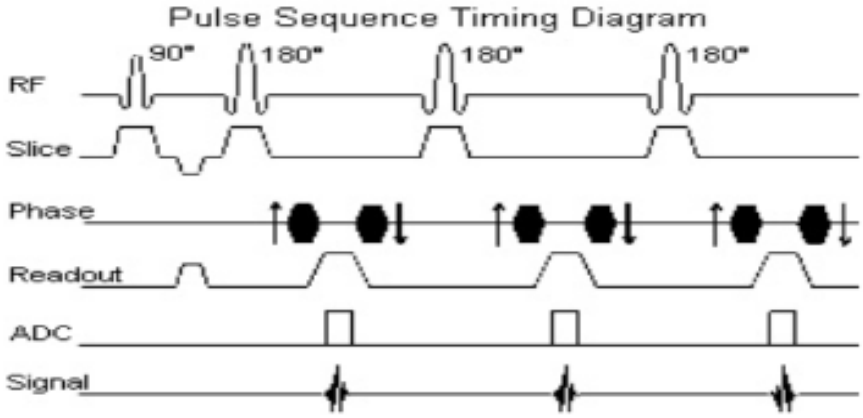


Figure 3.19: The Fast Spin echo sequence [Curtsy of J. E. Tanner & E. O. Stejskal "The Fast Spin-Echo Method"].

The echo time TE may vary from echo to echo in the echo train. The echoes in the center of the K-space (in the case of linear k-space acquisition) mainly produce the type of image contrast, whereas the periphery of K-space determines the spatial resolution.

### 3.5.3. The Gradient Echo Sequence

In a Gradient Echo (GRE) sequence, there is no 180° RF pulse. Instead a bipolar readout gradient (which is the same as the frequency-encoding gradient) is required to create an echo. The Gradient Echo results from applying a de-phasing gradient before the frequency-encoding or readout gradient. The goal of this de-phasing gradient is to obtain an echo when the readout gradient is applied and the data are acquired. The de-phasing stage of the readout gradient is in the inverse sign of the readout gradient during data acquisition. Moreover, its de-phasing effect is designed so that it corresponds to half of the de-phasing effect of the readout gradient during data acquisition. Consequently, during data acquisition, the readout gradient will re-phase the spins in the first half of the readout (by reversing the de-phasing effect of the de-phasing lobe), and the spins will de-phase in the second half (due to the de-phasing effect of the readout gradient). The time during which the peak signal is obtained is called Echo Time (TE).

The excitation pulse is termed the alpha pulse ‘α’. It tilts the magnetization by a flip angle ‘α’, which is typically between 0° and 90°. Gradient echo imaging is typically accomplished by examining the FID, whereas the read gradient is turned on for localization of the signal in the readout direction. The contrast and signal generated by a gradient echo depend on the size of the longitudinal magnetization and the flip angle. When α = 90° the sequence is identical to the so-called partial saturation or saturation recovery pulse sequence.

In standard GRE imaging, this basic pulse sequence is repeated as many times as image lines have to be acquired. Gradient echoes have a lower Specific Absorption Rate (SAR) than most spin echo sequences. SAR is defined as the RF power absorbed per unit of mass of an object, in W/kg. In practical terms this is a measure of how much RF energy is needed to produce images and varies from

sequence to sequence. Gradient Echo sequences are more sensitive to field in-homogeneities and have a reduced crosstalk, so that a small or no slice gap can be used. As the flip angle is decreased, T1 weighting can be maintained by reducing the TR. In a standard Gradient Echo Sequence, pure T2 weighting is not possible, however, T2* images can be obtained by keeping the TE as short as possible. A Gradient Echo is generated by using a pair of bipolar gradient pulses (Fig. 3.20). There is no refocusing 180° pulse as in the basic Spin Echo sequence and the data are sampled (ADC) during a Gradient Echo, which is achieved by de-phasing the spins with a negatively pulsed gradient before they are re-phased by an opposite gradient with opposite polarity to generate the echo.

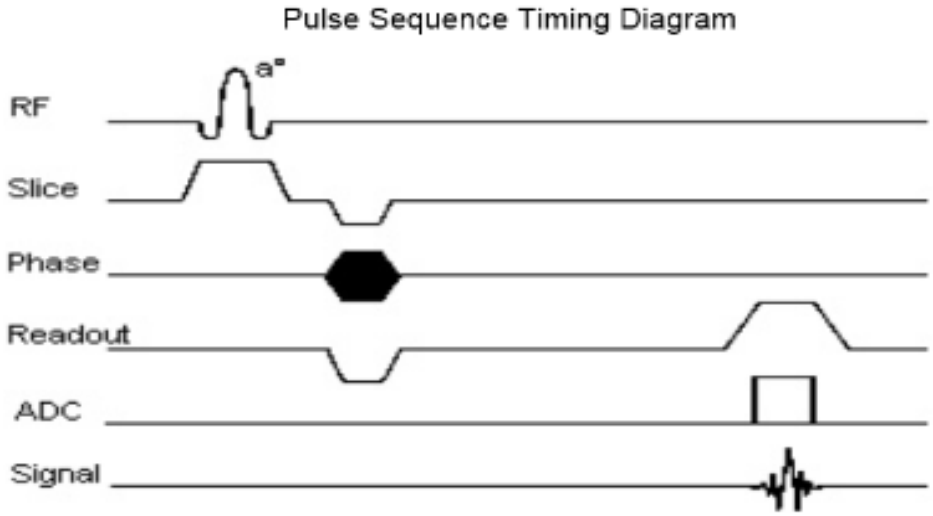


Figure 3.20: Gradient Echo Sequence Diagram [Curtsy of J. E. Tanner & E. O. Stejskal "The Gradient-Echo Method"].

What is the difference between T2 and T2*? In idealized nuclear magnetic resonance experiment, the FID decays approximately exponentially with a time constant T2, but in practical MRI small differences in the static magnetic field at different spatial locations (“in-homogeneities”) cause the Larmor frequency to vary across the body creating destructive interference which shortens the FID. The time constant for the observed decay is the T2* relaxation time, and is always shorter than T2.

# Chapter 4. Medical Image Processing

## 4.1. Introduction

Medical imaging has experienced tremendous progress during the past decade and image processing is a rapidly growing area of information technology. Its growth has been fueled by technological advances in digital imaging, computer processors and mass storage devices [50]. Digital images are composed of individual *pixels* (this acronym is formed from the words “picture” and “element”), to which discrete brightness or color values are assigned. They can be efficiently processed, objectively evaluated, and made available at many places at the same time by means of appropriate communication networks and protocols, such as Picture Archiving and Communication Systems (PACS) and the Digital Imaging and Communications in Medicine (DICOM) protocol. Based on digital imaging techniques, the entire spectrum of digital image processing is now applicable in medicine [42].

Biomedical image processing deals with the development of problem-specific approaches to the enhancement of raw medical image data for the purposes of selective visualization as well as further analysis [4]. It has experienced dramatic expansion, and has been an interdisciplinary research field attracting expertise from applied mathematics, computer sciences, engineering, statistics, physics, biology and medicine [48]. As a result of that, computer-aided diagnostic processing has already become an important part of clinical routine [4].

## 4.2. Steps of Image Processing

The commonly used term “biomedical image processing” means the provision of digital image processing for biomedical sciences. In general, digital image processing covers four major areas [42] and are summarized in Fig. 4.1.

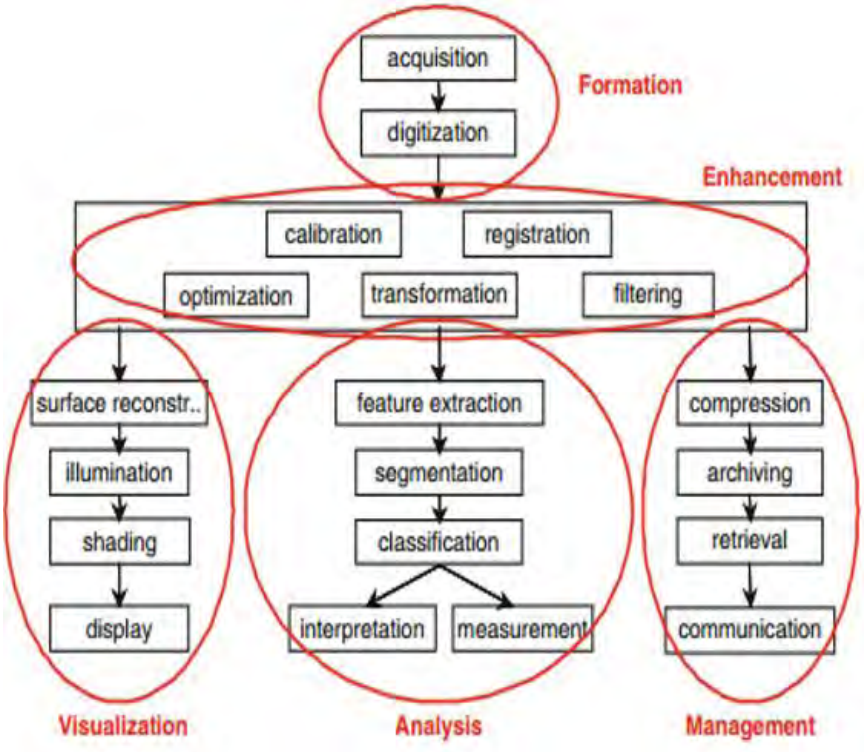


Figure 4.1: Modules of image processing covers four main areas:

- image formation
- visualization
- analysis, and
- management.

The algorithms of image enhancement can be assigned as pre and post-processing in all areas [42].

[Curtsy of T. M. Deserno, Biomedical Image Processing, Biological and Medical Physics]

1. *Image formation* includes all the steps from capturing the image to forming a digital image matrix [42].
2. *Image visualization* refers to all types of manipulation of this matrix, resulting in an optimized output of the image [42].
3. *Image analysis* includes all the steps of processing, which are used for quantitative measurements as well as abstract interpretations of biomedical images. These steps require a priori knowledge on the nature and content of the images, which must be integrated into the algorithms on a high level of abstraction. Thus, the process of image analysis is very specific, and developed algorithms can be transferred rarely directly into other application domains.
4. *Image management* sums up all techniques that provide the efficient storage, communication, transmission, archiving, and access (retrieval) of image data. Thus, the methods of telemedicine are also a part of the image management.

While an MRI system is rather complex, the underlying imaging principles of such a system are rather straight forward, especially from the signal processing point of view. The imaging process involves forward and inverse Fourier transforms as shown in Fig. 4.2 below [49].

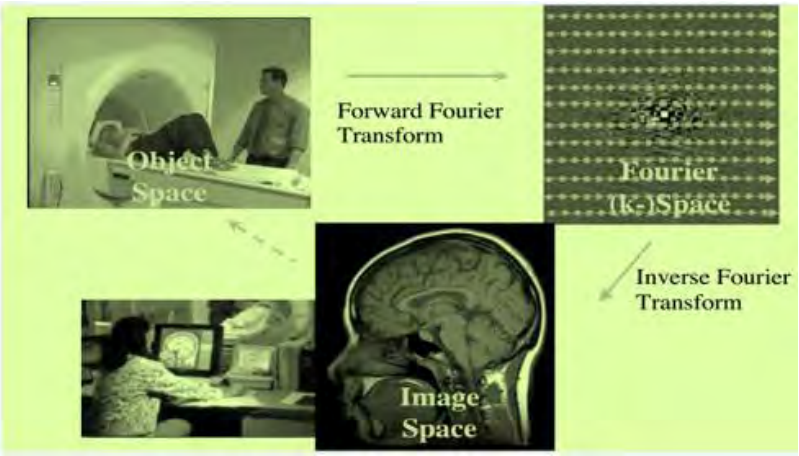


Figure 4.2: The MR imaging process can be viewed as forward and inverse Fourier transforms [Curtsy of Medical Image Processing Overview Hongmei Zhu, University of Calgary PP.2]

## 4.3. Color Image Processing

Color image is defined as a three-dimensional array and consisted of three, two dimensional arrays called voxels (dimensions of 3D volume that are parallel), one for the red component, the second for the green component and the third for blue component [42]. Each voxel on such color images can be represented as a three component vector and analogously, an MRI voxel can be seen as a vector with as many channels as available MR image parameters such as T1, T2 and PD/ADC. In this regard, the idea of color image processing has been an important part of MP-MRI processing systems. This principle has been particularly applied in identification of clear boundary of tumorous tissues from the healthy background [33]. Other known applications include image denoising, object enhancement, segmentation and the like [1].

One peculiar characteristic of most of the color image processing tools currently available in the literature is the need of color component separation (say in case of RGB into red, blue and green components) in order to get the gray (monochromatic) equivalent of the color image. Traditionally, each monochrome will then be processed using one or more image processing techniques, and later

combined to form a processed color image [10]. But this idea of converting a color image to gray or into its monochromatic components, apply image processing on the resulting monochromes, and then combine back/convert the processed images back to a color image has known draw backs: the first could be the loose of the intrinsic inter-correlation information embedded among the monochromes, which is particularly important in applications such as texture and pattern recognition. Second issue is that there is no known (trivial) tool to convert back the processed gray components to a color. Another issue is the considerable computational cost both in terms of processing time as well as storage [4, 37]. In this regard, a holistic approach should result in an effective color processing as well as optimized scheme. The holistic approaches treat each color voxel as a single object/entity and the processing is done accordingly. One such approach which has gained a lot of attention recently uses vectorial schemes (vectorial color image processing) which makes use of Clifford algebras, such as quaternions, and related Fourier transforms [1, 2]. A gray scale image is composed of varying intermediate shades of gray ranging from black to white. For example, the commonly used 8-bit gray scale image is composed of 2^8 = 256 shade gray scale, where a value of 0 represents a pure black color, the value of 255 represents pure white and each value in between represents a progressively darker shade of gray.

Objects in a gray tone display have a brightness value (or digital number), which represents the measured energy level of the item. The difference in the relative brightness between an item and its surroundings as seen in the image is what we call contrast. A particular feature is easily detected in an image when contrast between an item and its background is high. However, when the contrast is low, an item might go undetected in an image. As opposed to their gray scale/monochromatic counterparts, color images are made of multiple channels/bands/components. It could be one of the followings: a true color image, a pseudo color, or a false color.

In true colors of an object an image appears to a human observer the same way as if this observer were to directly view the object: A green tree appears green in the

image, a red apple red, a blue sky blue, and so on. A true color image is one for which the colors have been assigned to digital number values that represent the actual spectral range of the colors used in the image (blue features appear blue, green features appear green, red features appear red). A photograph is an example of a true color image. Graphics file formats often store RGB images as 24 bit images, where the red, green and blue components are 8 bits each. This yields a potential of more than 16 million colors (256^3). The precision with which a real-life image can be replicated has led to the nickname "true color image" [25].

False-color is any representation that does not show the true colors of the subject as they would appear to the eye. It is an image (as a photograph) of an object that does not actually appear in the object but is used to enhance, contrast, or distinguish details. Pseudo-color image processing consists of assigning colors to gray values based on a specified criterion. The term “pseudo-color” emphasizes that the colors were assigned artificially opposing to the true (real) colors.


Figure 4.3: Examples of overlaying additional information with pseudo color [Curtsy of https://en.wikipedia.org/wiki/Pseudo_color]

The principal use of pseudo-colors is for human visualization and interpretation of gray scale details on an image or their sequence. Pseudo-coloring can make some details more visible, as the perceived difference in color space is bigger than between successive gray levels alone.

For true color, the RGB channels (red "R", green "G" and blue "B") from the camera are mapped to the corresponding RGB channels of the image, yielding a "RGB→RGB" mapping. For false color this relationship is changed. The simplest false-color encoding is to take an RGB image in the visible spectrum, but map it differently, e.g. "GBR→RGB".

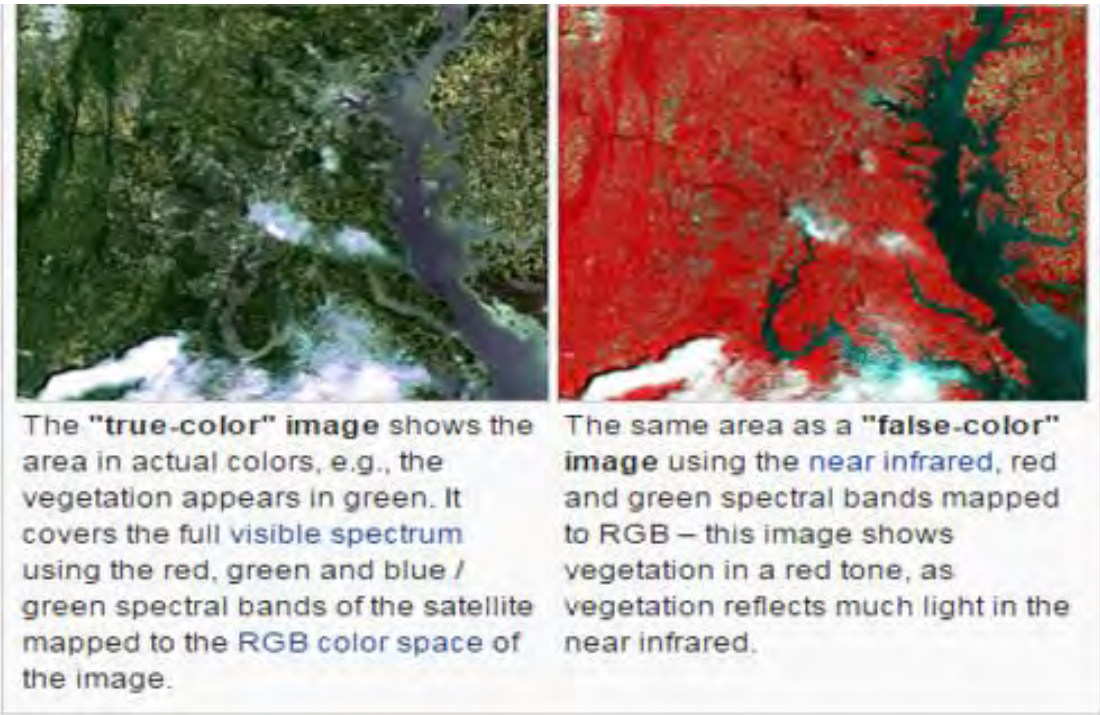


Figure 4.4: Two exemplary Landsat satellite images showing the same region: Chesapeake Bay and city of Baltimore [Curtsy of https://en.wikipedia.org/wiki/False_color]

Most raw pictures are stored in a gray scale format. A gray scale is a color scale that ranges from black to white, with varying intermediate shades of gray. A commonly used gray scale for remote sensing image processing is a 256 shade gray scale, where a value of 0 represents a pure black color, the value of 255 represents pure white and each value in between represents a progressively darker shade of gray.

## 4.4. Color Models: Overview

### A. RGB color model

An RGB image, sometimes referred to as a “true color” image, can be stored as an m-by-n-by-3 data array that defines red, green and blue color components for each individual color pixel. The color of each pixel is determined by the

combination of the red, green and blue intensities stored in each color plane at the pixel's location [33].

The colors of the RGB model can be described as a triple (R, G and B). The RGB color space can be considered as a three-dimensional unit cube, in which each axis represents one of the primary colors as shown in Fig. 4.5 and the colors are points inside the cube defined by its coordinates. The primary colors thus are represented as red = (1, 0, 0); green= (0,1,0) and blue = (0,0,1). Similarly, the secondary colors are represented as cyan = (0, 1, 1), magenta = (1, 0, 1) and yellow = (1, 1, 0). Note that we used a unit cube to represent the RGB space after normalization. Otherwise, for an 8-bit representation for example, a red corresponds to the coordinate (255,0,0) and similarly for the other components. From now on, unless specified, we use this normalized representation for the successive discussions. The colors are often normalized as given below and this normalization guarantees that r + g + b = 1 [33].

$$r = \frac{R}{(R+B+G)}, g = \frac{G}{(R+B+G)}, b = \frac{B}{(R+B+G)} \tag{4.1}$$

The nature of the RGB color system is additive in the sense how adding colors makes the image brighter. Black is at the origin and white is at the corner where R = G = B = 1. The gray scale extends from black to white along the line joining these two points (the grey line) [29]. Thus a shade of gray can be described by the triplet (x, x, x) starting from black = (0, 0, 0) to white = (1, 1, 1).

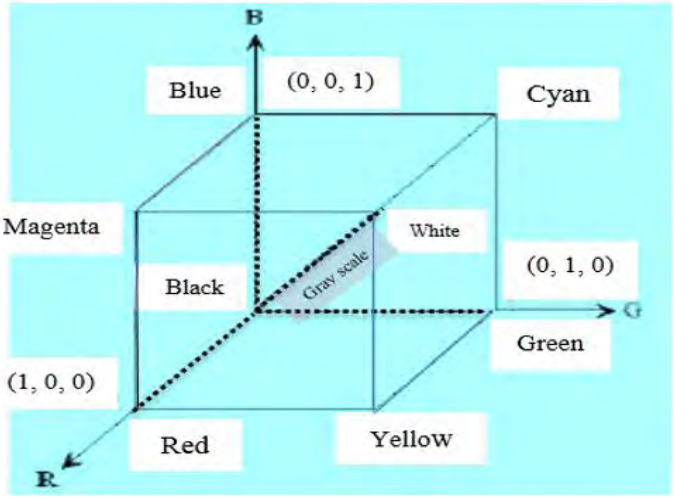


Figure 4.5: RGB and CMY color cube [Curtsy of https://en.wikipedia.org/wiki/RGB_color_model]

### B. CMY Color Model

The CMY color model is closely related to the RGB model. Its primary colors are C (cyan), M (magenta) and Y (yellow). i.e., the secondary colors of RGB are the primary colors of CMY and vice versa. The RGB to CMY conversion can be performed easily by [25]:

$$C = 1-R$$

$$M = 1-G$$

$$Y = 1-B$$

The CMY color system is often used in offset printing in a subtractive way, contrary to the additive nature of RGB. A pixel of color cyan, for example, reflects all other RGB colors but red. A pixel with the color of magenta, on the other hand, reflects all other RGB colors but green. Now, if we mix cyan and magenta, we get blue, rather than white like in the additive color system.

### C. HSI Color Model

The HSI model consists of hue (H), saturation (S) and intensity (I). Intensity corresponds to the luminance component. Hue is an attribute associated with the dominant wavelength in a mixture of light waves, i.e., the dominant color as perceived by an observer. Saturation refers to relative purity of the amount of white light mixed with hue [29].

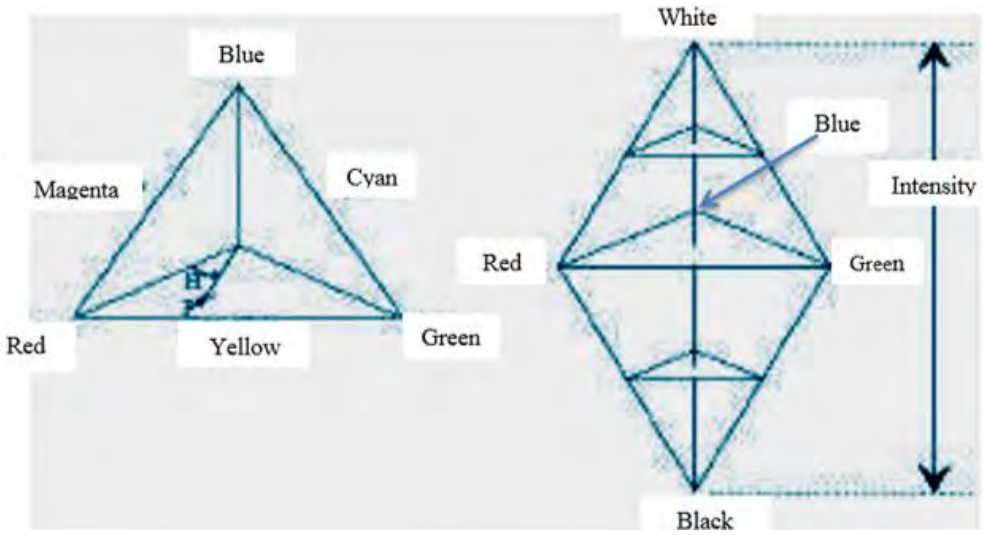


Figure 4.6: HSI color Triangle (left); HSI color solid (right) [Curtsy of https://en.wikipedia.org/wiki/HSI_color_space]

The advantages of HSI are:

- The intensity is separated from the color information
- The hue and saturation components are intimately related to the way in which human beings perceive color.

Whereas RGB can be described by a three-dimensional cube, the HSI model can be described by the color triangle shown in Fig. 4.6. All colors lie inside the triangle whose vertices are defined by the three initial colors. If we draw a vector from the central point of the triangle to the color point P shown on the figure, then Hue (H) is the angle of the vector with respect to the red axis. For example 0° indicates red color, 60° yellow, 120° green and so on.

Saturation (S), which is the degree to which the color is undiluted by white, is proportional to the distance to the center of the triangle.

Given an RGB color image, the HSI equivalent can be computed as follows:

$$\mathrm{H} = \frac{1}{360^o}\cos^{-1}\left[\frac{\frac{1}{2}[(\mathrm{R}-\mathrm{G})+(\mathrm{R}-\mathrm{B})]}{\sqrt{(\mathrm{R}-\mathrm{G})^2+(\mathrm{R}-\mathrm{B})(\mathrm{G}-\mathrm{B})}}\right], \text{ If B>G} \qquad (4.2)$$

$$\mathrm{H} = 1 - \frac{1}{360^o}cos^{-1}\left[\frac{\frac{1}{2}[(R-G)+(R-B)]}{\sqrt{(R-G)^2+(R-B)(G-B)}}\right], \text{ Otherwise.} \qquad (4.3)$$

$$\mathrm{S} = 1 - \frac{3}{(\mathrm{R}+\mathrm{G}+\mathrm{B})}\min(\mathrm{R},\mathrm{G},\mathrm{B}) \qquad (4.4)$$

$$I = \frac{1}{3}(R+G+B) \qquad (4.5)$$

The steps used to convert an RGB image to HSI image model and back to RGB model are briefly summarized below:

- Get the normalized red, green and blue components from the RGB

$$\mathrm{r} = \frac{\mathrm{R}}{\mathrm{R}+\mathrm{G}+\mathrm{B}}, \mathrm{g} = \frac{\mathrm{G}}{\mathrm{R}+\mathrm{G}+\mathrm{B}}, \mathrm{b} = \frac{\mathrm{B}}{\mathrm{R}+\mathrm{G}+\mathrm{B}} \qquad (4.6)$$

- Calculate the H, S and I components by applying the following:

$$\mathrm{H} = \cos^{-1}\left[\frac{0.5[(\mathrm{r}-\mathrm{g})+(\mathrm{r}-\mathrm{b})]}{[(\mathrm{r}-\mathrm{g})^2+(\mathrm{r}-\mathrm{b})(\mathrm{g}-\mathrm{b})]^{\frac{1}{2}}}\right]; \text{If } \mathrm{H}\epsilon[0,\pi] \text{ for } \mathrm{b} \leq \mathrm{g} \qquad (4.7)$$

and

$$H = 2\pi - \cos^{-1}\left[\frac{0.5[(r-g)+(r-b)]}{[(r-g)^2+(r-b)(g-b)]^{\frac{1}{2}}}\right]; \text{If } H\epsilon[\pi, 2\pi] \text{ for } b > g$$

S=1-3min(r,g,b); S∈ [0,1] (4.8)

$$I = \left(\frac{R+G+B}{3.255}\right);\ I \in [0,1]$$

- Process the I component:
- Apply inverse conversion using the following

$$h = H\frac{\pi}{180};\ s = \frac{S}{100};\ i = \frac{I}{255} \quad (4.9)$$

$$x = i(1-s)$$

$$y = i\left[1 + \frac{s\cos(h)}{\cos(\frac{\pi}{3}-h)}\right]$$

$$z = 3i - (x+y)$$

Example: Suppose we have a true-color pixel with the values 100 for the red, 150 for the green and 200 for the blue color:

- Find the components:

$$r = \frac{R}{R+G+B} = 0.222;\ g = \frac{G}{R+G+B} = 0.333;\ b = \frac{B}{R+G+B} = 0.444 \quad (4.10)$$

Here b>g; so

$$h = 2\pi - cos^{-1}\left[\frac{0.5[(r-g)+(r-b)]}{[(r-g)^2+(r-b)(g-b)]^{\frac{1}{2}}}\right] \quad (4.11)$$

$$= 1.167\pi$$

$$S = 1 - 3\min(r,g,b) = 0.333 \quad (4.12)$$

Find H, S and I;

H = 180h = 210

S = 100s = 33.3

I = $\frac{R+G+B}{3}$ = 150

Apply inverse conversion

$$h = \frac{H}{180} = \frac{7}{6} \quad (4.13)$$

$$s = \frac{S}{100} = 0.333 \quad (4.14)$$

$$i = \frac{I}{225} = 0.588 \quad (4.15)$$

### D. YIQ Color Model

YIQ is a slightly different version of YUV. It is mainly used in North American television systems. Here Y is the luminance component, just as in YUV. I and Q correspond to U and V of YUV color systems. The RGB to YIQ conversion can be carried our using the following formula:

$$Y = 0.299R + 0.587G + 0.114B \quad (4.16)$$

$$I = 0.596R - 0.275G - 0.321B \quad (4.17)$$

$$Q = 0.212R - 0.523G + 0.311B \quad (4.18)$$

The YIQ color model can also be described corresponding to YUV:

$$Y = 0.3R + 0.6G + 0.1B \quad (4.19)$$

$$I = 0.74V - 0.27U \quad (4.20)$$

$$Q = 0.48V + 0.41U \quad (4.21)$$

### E. YUV Color Model

The basic idea in the YUV color model is to separate the color information apart from the brightness information. The components of YUV are:

$$Y = 0.3R + 0.6G + 0.1B \quad (4.22)$$

$$U = B - Y \quad (4.23)$$

$$V = R - Y \quad (4.24)$$

Y represents the luminance of the image, while U and V consists of the color information, i.e., chrominance. The luminance component can be considered as a gray-scale version of the RGB image. The advantages of YUV compared to RGB are:

- The brightness information is separated from the color information;
- The correlations between the color components are reduced;
- Most of the information is collected to the Y component, while the information content in the U and V is less.

The latter two properties are beneficial in image compression. This is because the correlations between the different color components are reduced, thus each of the components can be compressed separately. Besides, more bits can be allocated to the Y component than to U and V. The YUV color system is adopted in the JPEG image compression standard.

### F. Lab Color Model

The color space defined by the Lab is based on one channel for Luminance (lightness) (L) and two color channels (a and b). One problem with the XYZ color system, is that colorimetric distances between the individual colors do not correspond to perceived color differences. The Lab color space includes all perceivable colors, which means that its gamut exceeds those of the RGB and CMYK (K stands for black) color models. This means unlike the RGB and CMYK color models, Lab color is designed to approximate human vision. It aspires to perceptual uniformity, and its L component closely matches human perception of lightness. One of the most important attributes of the Lab model is device independence. This means that the colors are defined independent of their nature of creation or the device they are displayed on.

## 4.5. Image Segmentation: Overview

Image segmentation is defined as partitioning of an image into regions that are meaningful for a specific task; it is a labeling problem. This may, for instance, involve the detection of a brain tumor from MR or CT images (see Fig. 4.7 for example). Segmentation is generally considered one of the first steps leading to effective image analysis and interpretation [13].

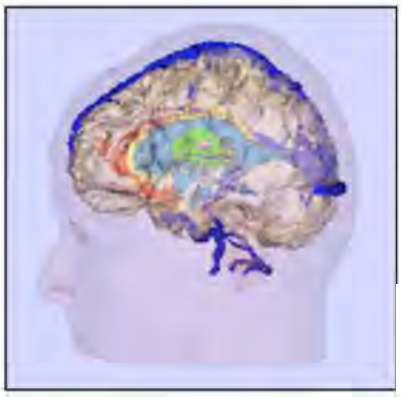

Figure 4.7: A 3D rendering of segmented skin surface (pink), brain tissue (brown), major blood vessel (navy blue), and a tumor (green) from MRI volume. This allows surgeon to visualize the actual location and to plan and simulate specific **Procedures [Curtsy of Medical Image Processing Overview Hongmei Zhu, University of Calgary PP.2]**

The principal goal of the segmentation process is to partition an image into regions (also called clusters, or subsets) that are homogeneous with respect to one or more characteristics or features or having strong correlation with areas of interest in the image which is an important tool in medical image processing and it has been found useful in many applications [49]. Therefore, image segmentation is the

core concept of image processing. Image segmentation approaches can be classified according to both the features and the type of techniques used. Features include, for example, pixel intensities, edge information, texture, and the like. Techniques based on these features can be broadly classified into structural and statistical methods. Structural methods are based on the spatial properties of the image, such as edges and regions [22].

Region growing is one popular structural technique. In this approach, one begins by dividing an image into small regions, which can be considered as “seeds”. Then, all boundaries between adjacent regions are examined. Strong boundaries (in terms of certain specific properties) are kept, while weak boundaries are rejected and the adjacent regions merged. The process is carried out iteratively until no boundaries are weak enough to be rejected. However, the performance of this method depends on seed selection and whether the regions are well defined, and therefore is often times not considered robust [37]. Starting from a totally different viewpoint, statistical methods label pixels according to probability values, which are determined based on the intensity distribution of the image [39]. Gray-level thresholding is the simplest, yet often effective segmentation method. In this approach, structures in the image are assigned a label by comparing their gray-level value to one or more intensity thresholds. A single threshold serves to segment the image into only two regions, a background and a foreground, as illustrated in Fig. 4.8 [39]. Sometimes the task of selecting a threshold is quite easy, when there is a clear difference between the gray-levels of the objects we wish to segment. But generally speaking, picking the right threshold to segment an arbitrary image could be very challenging, and the complexity is even more pronounced for medical images.

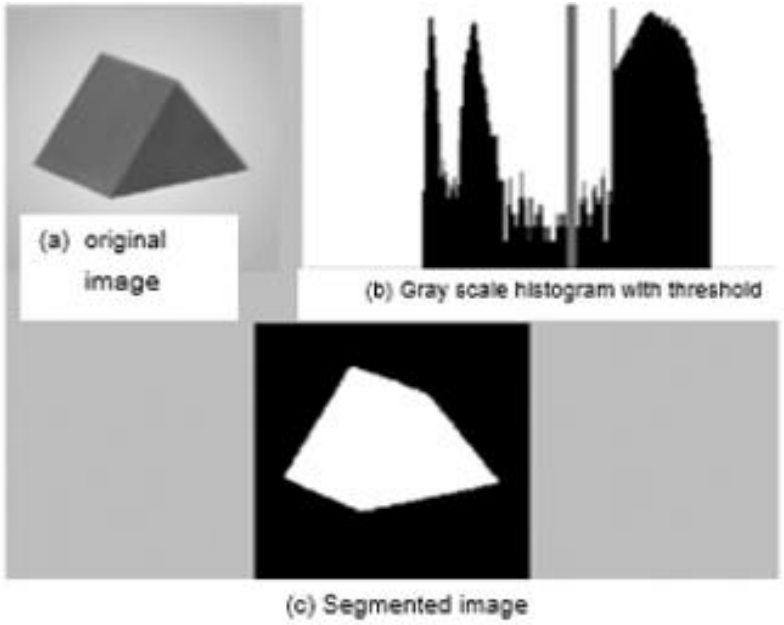


Figure 4.8: Segmenting a simple image by a single threshold

**[Curtsy of Medical Image Processing Overview Hongmei Zhu, University of Calgary PP.22]**

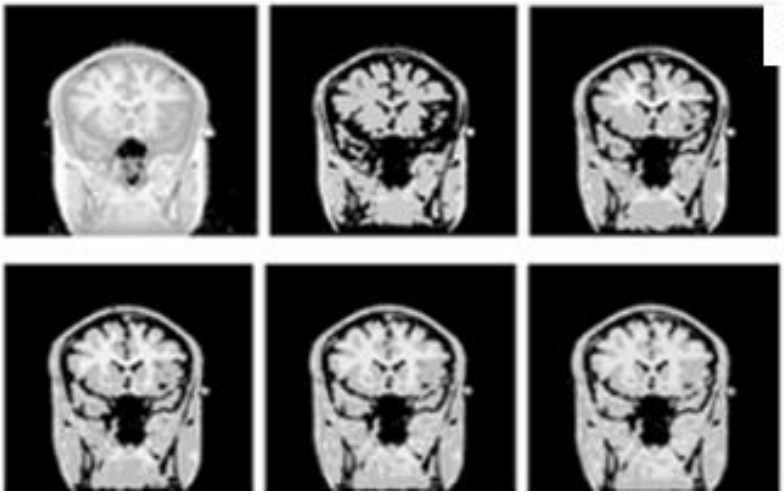

Figure 4.9: Top to bottom, left to right: Input image and tissue classification generated by successive iterations of the EM segmentation (WM is brightest, GM is medium grey, and CSF and air are black). Bottom right is the final segmentation.

Another important method used in segmentation is texture analysis. Texture is basic cue for human beings to recognize objects [57]. Texture analysis, for use in such as segmentation and classification, plays a vital role in computer vision and pattern recognition and is widely applied to many areas such as industrial automation, bio-medical image processing, texture synthesis, shape, remote sensing, and the like [57].

## 4.6. Image Features for Brain Tumor Segmentation

The features used for segmentation of brain tumors largely depend on the type of tumor and its grade because different tumor types and grades can vary a lot in appearance (e.g. contrast uptake, shape, regularity, location, etc.). Additionally,

feature selection will also depend on the sub compartment of the tumor, which is to be segmented. The most common features used for brain tumor segmentation are the image intensities. This is based on the assumption that different tissues have different gray levels [25].

Other types of features frequently used are local image textures because it has been observed that different tumor areas exhibit different textural patterns [63]. Textures can be computed based on different strategies as shown in [64]. Others are alignment-based features which make use of spatial prior knowledge, which is often encoded by registration of a standard atlas to the patient image or by making use of symmetries between left and right brain hemisphere. Intensity gradients or edge-based features can be used for evolving a contour towards the tumor border. Recently, context-aware features modeling mid- or long-range spatial contexts similar to the one suggested in [65] are becoming more popular. Depending on the data available, all these features can either be computed from one single modality or from multi-modal images.

Researchers have also combined different features from different modalities in order to improve their segmentation results. For the task of brain tumor image analysis, authors in [50] explored different features for voxel-based classification and concluded that combining textural and alignment-based features allowed for substantial performance increases. In [50], the authors investigated the efficacy of different image features and feature fusion strategies for pediatric brain tumor images. They argued that in multi-modal images, texture features had advantages over intensity or shape features.

## 4.7. MR-Image Preprocessing and Re-construction

Since most of the real life data is noisy, inconsistent and incomplete, preprocessing becomes necessary. Image pre-processing is one of the preliminary steps which are highly required to ensure the high accuracy of the subsequent steps. The raw MR images normally consist of many artifacts such as intensity in-homogeneities, cranial tissues, and patient motions during image acquisition, thermal noise and existence of metallic materials in imaging environment and film artifacts or label on

the MRI such as patient name, age and marks which reduces the overall accuracy. So such artifacts need to be removed by pre-processing procedures prior to further analysis [57].

## 4.8. Image Registration

Image registration is the process of transforming the different sets of image data into one coordinate system. Registration is necessary in order to be able to compare or integrate the data obtained from different measurements. A diagram illustrating the major blocks of most registration pipelines is shown in the Fig. 4.10.

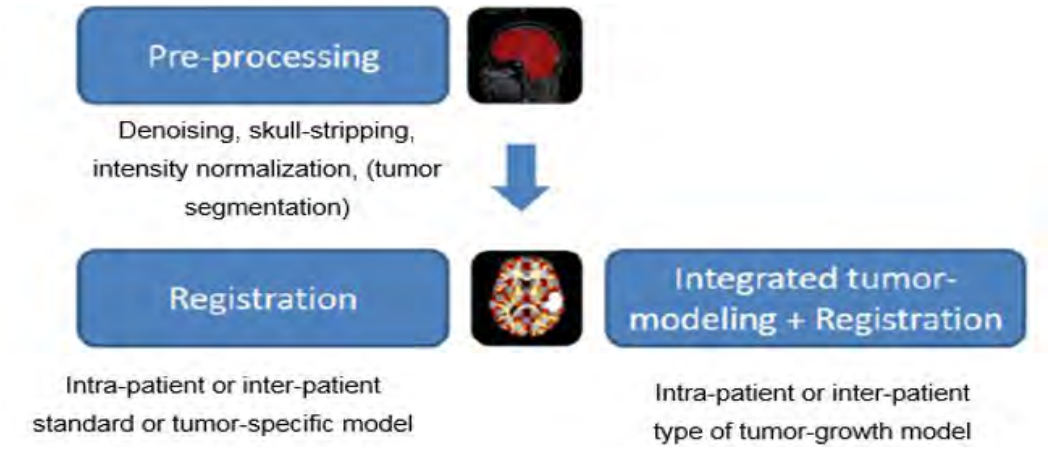


Figure 4.10: Illustration of the main blocks, which are used for building up the registration pipeline of most algorithms [Curtsy of https://en.wikipedia.org/wiki/Color_image_pipeline]

Medical image registration (e.g. for data of the same patient taken at different points in time) often additionally involves elastic (or non-rigid) registration to cope with deformation of the subject (due to breathing, anatomical changes, etc.).

Image registration of tumor-bearing brain images mainly focuses on two different objectives: intra-patient multi-modal or longitudinal registration (alignment) of images on the one hand, and inter-patient spatial normalization of brain tumor images to a brain atlas on the other hand [66].

Other than the standard registration methods, there are also methods integrating tumor-growth modeling with registration. Again, both can be sub-grouped into intra- or inter-patient methods, which can use either standard or tumor-specific registration algorithms. Usually, an initial rigid alignment is followed by a non-rigid

transformation step [50]. The feature metric, which is used by most approaches, is intensity-based registration due to its general applicability [49]. Most algorithms perform a linear registration for initial alignment before a non-rigid transformation is applied. The non- rigid transformation can be standard or tumor-specific.

## 4.9. MRI Image Re-construction

To obtain MRI images we need two things:

1) Information about differences in tissue (image contrast), this is obtained by utilizing differences in tissue T1 and T2 behavior.
2) Information about from where the signal is coming from in the target (image resolution).

These two are obtained by using a combination of RF pulses and additional, time and distance varying magnetic fields called gradient fields. This combination of RF pulses and gradient fields is termed an imaging sequence.

# Chapter 5. Automatic Brain Tumor Detection based on Holistic MP-MRI Analysis

## 5.1. Introduction

The development of automatic systems for medical image processing, which can effectively act as an agent to aid medical diagnosis, is a goal that has been pursued by researchers since the first works on the field of medical image processing. The automation of image analysis tasks can produce very interesting results such as less time spent by specialists, decrease of intra-and inter-observer differences, second opinions to non-specialists and in educational systems among other things [48]. However, the automatic identification of structures is a research area of image processing that still has great challenges.

As said before, one thing that is often considered a tremendous advantage of using MR imaging is the ability to generate different MR parameters, where each of them have their own specific merits. These parameters, offering distinct information about the same object, are essentially correlated to each other. A clever image analysis tool should then be able to exploit this information to reveal useful information as well as extract powerful imaging features. Such inter-correlations, which are traditionally accessed in individual (serial) processing mode, can be analytically discovered by crossbreeding the separate complement parameters into single color image, so called Multi-parametric MRI (MP-MRI) processing. To date various techniques have been developed for efficient analysis of multi-spectral medical images, specifically MP-MR images. Particularly, in this thesis we are interested in those novel approaches which apply color principles [1, 2] after representation of the MP-MR images in suitable higher order algebraic spaces.

## 5.2. Multi-Parametric Magnetic Resonance Imaging (MP-MRI)

We have talked about image processing based on one single MR image. However, MRI data are by nature multi-spectral because their contrast characteristics depend on the acquisition sequences and their parameters. As an example, Fig. 5.1 shows proton density weighted, T2-weighted, T1-weighted, and gadolinium-

DTPA enhanced T1w (GAD) brain MRI scans of the same multiple sclerosis (MS) patient. Extracting data from multispectral MR exams may provide us additional useful information in disease diagnosis and treatment assessment [7].

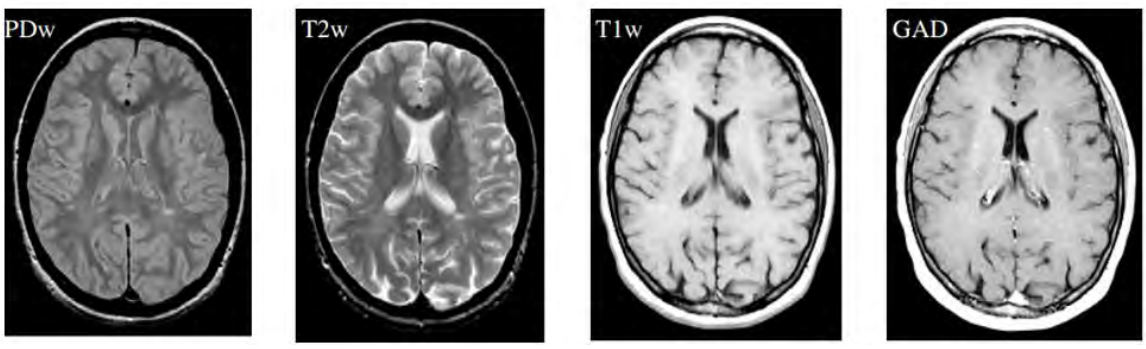


Figure 5: Example of multi-spectral MR images. From left to right: Proton density weighted, T2 weighted and gadolinium enhanced T1W (GAD) brain MRI scans of the same MS patient [Curtsy of Medical Image Processing Overview Hongmei Zhu, University of Calgary PP.42)

The inability of structural MRI to accurately measure tumor response to therapy complicates care management for patients with gliomas. Particularly for use in cancer research, several innovative ideas have been embraced in the current MR technology. Relaxation based as well as functional MRI techniques reveal detailed anatomical and physiological information of interest. Particularly in case of gliomas, multi-parametric MR imaging provides vast amount of information about anatomical, functional and metabolic characteristics [7].

MRI generates multi-parametric data because of its unique ability to form images influenced by different types of tissue parameters (i.e. proton density–weighted imaging, T2WI, T1WI, and DWI) [6]. In addition, by using these MR images, an n-dimensional feature space can be constructed by plotting each MR image on a separate axis. In particular, unsupervised segmentation methods, such as K-means and fuzzy c-means, can be applied to multi-parametric MRI data for exploratory clustering and analysis [7].

The combination (addition) of quantitative T1, T2, and ADC/PD-MRI to a clinical protocol provides some insight into the underlying physiology or structure of the tissue, contributing to discrimination of malignant versus normal tissue. Multi-parametric MRI is hence impacted by the strengths and weaknesses of each

individual parameter and often provides good performance for identifying malignant voxels in the peripheral zone.

A sequence of MR image parameters of the same anatomical site contains information pertaining to the tissue parameters. This implicit information may be used for image analysis and tissue characterization. The multi-parametric MRI data (in our case T1W, T2W and ADC/PD) provide complementary information about the status of the tissue. Most previous attempts to analyzing such MP-MR images, however, focused on processing each separate component serially and combining the outputs from the different channels without considering the intrinsic correlation between the components. The issue now is that there can be no simple way to correlate the resulting outputs and it is believed that exploiting the inter correlation information is vital in many image processing applications [2, 7]. In this regard, more holistic methods that treat sequence of MRI parameters as one entity retaining the correlation information have been suggested. One such an approach makes use of vectorial representations of the different MRI parameters [1, 2].

The vectorial approaches combined with the concept of color processing have been used previously in efficient analysis of MP-MR images [1, 7]. Particularly the use of Clifford algebra and its variants together with the respective integral transforms are considered novel approaches to study multi-channel images and it is the main intent of the current study to discuss uses of such multi-dimensional integral transforms in analysis of MP-MR images as colors with multiple channels.

## 5.3. Holistic MP-MRI Methodologies

One possible design for a holistic representation and analysis of multi-parametric MR images without masking the intrinsic inter-correlation among the different parameters makes use of vectors [1, 2, 7]. By use of schemes developed based on such vectorial image representations, one can combine different MR image parameters as one color image represented in a suitable color space for the purposes of enhancing structures and hence can be used for various research purposes with as many clinical implications.

The novel idea is treatment of MP-MR images as three component colors sitting in a suitable color space. Most color images have three components and each voxel on such color images can be represented as a three component vector. Analogously, an MRI voxel can be seen as a vector with as many channels as available MR image parameters: T1, T2, ADC, rCBV, Ktrans, T2*, etc. We might, for example, be interested in image processing such as de-noising, or other tasks such as object enhancement, segmentation or the like, based on a combination of different MRI parameters. Nevertheless, even a simple filtering operation applied on such multi component images is not always trivial as it is generally a non-linear process, which may not be carried out monochromatically but can benefit from vectorial approaches.

There was a recent study [1, 2] that proposed a promising application of color image transformations for efficient analysis of MP-MRIs. The work demonstrated the applicability of higher order Fourier transforms defined in both three (trinion) and four (quaternion) spaces in analyzing MP-MR images as multicolor images [1,2]. These higher dimensional numbers allow a vectorial representation of multi-component images and the respective Fourier transforms permit their analysis as one entity rather than separate monochromatic components. This thesis extends the concept and discusses details of the procedures used and some useful applications.

## 5.4. Holistic MP-MRI Analysis

There has been substantial advancement in analysis of multi-spectral images (or images with multiple bands/channels) since the introduction of holistic vectorial color image processing approaches which make use of Clifford algebras, such as quaternions, and related Fourier transforms [1, 2]. These higher dimensional numbers allow a vectorial representation of multi-component images and the respective Fourier transforms permit their analysis as one entity rather than detached monochromatic components [1]. This happens because information gained from these multi-parametric imaging techniques is largely complimentary and combinations of these compliments in these methods in to unity have been investigated successfully for glioma classification previously [3]. Some other

applications include color vector filtering, color image cross and auto-correlations to mention few. Note that the Clifford scheme using the Quaternions was first applied in grayscale image analysis inspired mainly by the symmetry of the quaternion Fourier transform [1, 2].

Generally, the analysis of multi-spectral/multi-color images in the Clifford space is getting a lot of attention recently. In that regard a novel quaternion and trinion based feature extraction scheme has been proposed recently for use in efficient tissue identification and classification of MP-MRIs [3,7]. Based on a holistic color processing concept, the work specifically tried to address a very challenging issue of automatic disease (tumor) identification making use of available multiple MR parameters.

## 5.5. Principal Component Analysis (PCA)

The Clifford way of color analysis also comes as a hybrid approach making use of other image processing techniques. One of these techniques is Principal Component Analysis (PCA) and is often referred to as a technique for reducing the number of variables in a data set without loss of information, and as a possible process for identifying new variables with greater meaning [11]. PCA is a linear transformation that has been applied in a variety of fields including MRI analysis [3]. It has been employed in digital image processing as a technique for image coding, compression, enhancement, and feature extraction. For MRI feature space representation, PCA generates linear combinations of the acquired images that maximize the image variance [5]. The number of principal component images equals the number of acquired images, but the variance (equivalently, the SNR) of the principal component images sharply decreases from the first image to the last. The first three principal component images often contain most of the information and can be used to define a feature space representation of the object (tissue in our case) under consideration.

## 5.6. Quaternion-Trinion Principles and Analysis: Overview

### 5.6.1. Quaternions and Quaternion Fourier Transforms

Quaternions were first introduced by Hamilton in 1843 [58]. The concept can sometimes be considered as a generalization of the natural complex numbers. A given complex number has two components: the real and the imaginary part. A quaternion instead has four components, i.e., one real and three imaginary parts and can be represented as [2]:

$$q = a + ib + jc + kd \tag{5.1}$$

where a, b, c and d are real numbers and i, j and k are orthonormal operators satisfying:

$$ij = k = -ji,\ jk = i = -kj,\ ki = j = -ik \tag{5.2}$$
$$\mathbf{i^2 = j^2 = k^2 = ijk = -1}$$

From these rules, it is clear that quaternion multiplication is not communicative. The quaternion conjugate is given by:

$$\bar{q} = a - ib - jc - kd \tag{5.3}$$

and the modulus of a quaternion is given by:

$$|\boldsymbol{q}| = \sqrt{a^2 + b^2 + c^2 + d^2} \tag{5.4}$$

A quaternion with zero real part is called a pure quaternion and a quaternion with unit modulus is called a unit quaternion. The imaginary part of a quaternion has three components and may be associated with a 3-space vector. For this reason, it is sometimes useful to consider the quaternion as composed of a vector part and a scalar part. Thus q can be expressed as [1, 2]:

$$q = S(q) + V(q) \tag{5.5}$$

where the scalar part, S(q) = a is the real part and the vector part is a composite of three imaginary components,

$$V(q) = ib + jc + kd \tag{5.6}$$

An RGB color triple for example is commonly represented as a pure quaternion of the form Ri + Gj + Bk. The Fourier transform, PCA and similar analysis techniques have already been extended to quaternion arithmetic [1] and we can use those for a clever analysis of our quaternion valued color images.

Quaternions provide a new way to process color and texture in combination. The advantage of the quaternion representation for color is that it combines a color 3-tuple (RGB or HSI) into a single hyper-complex number. A color can then be processed as a unit, rather than as 3 separate channels [2]. For example, a basis for the color textures occurring in a given image can be derived via quaternion principal component analysis of a training set of color texture samples. A color texture sample is then projected onto a subset of this basis to obtain a concise (single quaternion) description of the texture. The power of this quaternion color texture representation is then demonstrated by its use in an algorithm that successfully cluster textures and segments an image into regions of different textures [57].

## I. Some properties of quaternions

1. Quaternions form an associative, non-commutative four-dimensional algebra. Quaternion algebra is distinct from both real and complex algebra. For example, multiplication is not commutative in quaternion space. Here it is interesting to note the following exponential property in the quaternion space [1, 2].

$$e^{ib+jc} \neq e^{ib}e^{jc} \tag{5.7}$$

This shows that operations which are trivial in both real and Fourier spaces are not so obvious in the case of quaternions.

2. We can express a given quaternion number q as sum of a real part and a vector part as q = S(q)+V(q) where S(q) is the real part of the quaternion and V(q) contains the imaginary components.
3. Any quaternion, say q = a + ib + jc + kd, can be written in polar form as

$$q = |q|e^{\mu\phi} \tag{5.8}$$

where $|q| = \sqrt{a^2 + b^2 + c^2 + d^2}$ is called the amplitude (modulus), $\mu = \frac{V(q)}{|V(q)|}$ called eigen axis, and

$\emptyset = arctan\frac{|\boldsymbol{V}(\boldsymbol{q})|}{\boldsymbol{S}(\boldsymbol{q})}, 0 \leq \emptyset < \pi$ called Eigen angle (phase),

where $\mu \in Q$, $s(\mu) = 0, |\mu| = 1$ and $\mu^2 = -1$.

When, |μ| = 1 we call q a unit quaternion and when a=0, we call it pure quaternion. Euler's and De Moivre's formulae still hold in the quaternion space; i.e. for μ a unit quaternion the followings hold [1]:

$$(\cos(\theta) + \mu\sin(\theta))^n = e^{\mu n\theta} = \cos(n\theta) + \mu\sin(n\theta) \quad (5.9)$$

$$e^{\mu\emptyset} = \cos(\emptyset) + \mu sin(\emptyset)$$

4. Quaternion conjugate is given by $\bar{q} = a - ib - jc - kd$.
5. A complex number can be considered as a special quaternion number with one real and one imaginary part.
6. A quaternion is visualized in four space as opposed to the two-dimensional complex space.

Many more interesting properties of quaternions are found in different literatures and readers are advises to consult some of those.

## II. The quaternion Fourier transforms

Quaternion Fourier transforms (QFT) are fundamental tools in signal and image processing and play a vital role in the representation of two-dimensional signals and transformation into a quaternion-valued spatial frequency domain. It is a nontrivial generalization going from real and complex Fourier transforms to quaternion cases. The four QFT components separate four cases of symmetry in real signals instead of only two in the complex FT. Color image pixels have three components, and they can be represented in quaternion form using pure quaternions. For example, a pixel at image coordinates (n, m) in a RGB image can be represented as [1, 2]:

$$f(n,m) = r(n,m)i + g(n,m)j + b(n,m)k \quad (5.10)$$

where r(n, m) is the red component and g(n, m) and b(n, m) are the green and blue components of the pixel, respectively.

The same approach may be used with a luminance-chrominance color space, such as YCbCr. The choice of the imaginary part to represent pixel values is determined by interpretation of color pixels as vectors. The imaginary part of a quaternion has three components and may also be associated with a 3-space vector. This choice is not arbitrary, nor is it coincidental. One interpretation of a full quaternion is that it is the ratio of two vectors-that is, the quantity that multiplies one vector to give

another. This is a useful geometric interpretation that is exploited in the design of color image filters.

The non-commutative property of quaternions allows different forms of quaternion based integral transforms to be defined. The quaternion (or hyper-complex) Fourier transforms treats color images as vectors. The quaternion Fourier transform of type I is given by [1, 2]:

$$Q(k_x, k_y) = \iint_{-\infty-\infty}^{\infty\infty} e^{-\mu 2\pi(k_x x + k_y y)} f(x, y)\,dx\,dy \tag{5.11}$$

and its inverse is given by:

$$f(x, y) = \frac{1}{4\pi^2} \iint_{-\infty-\infty}^{\infty\infty} e^{\mu 2\pi(k_x x + k_y y)} Q(k_x, k_y)\,dk_x\,dk_y \tag{5.12}$$

where μ is any unit pure quaternion, $\mu^2 = -1$ and f(x, y) is generally quaternion valued. The Fourier transform is a special case in which μ = i. The parameter μ is chosen arbitrarily. For an RGB color image f(x, y) for example, where the image has three components which can be written as a quaternion as

$$f(x, y) = R(x, y)i + G(x, y)j + B(x, y)k \tag{5.13}$$

We customarily use $\mu = \frac{i+j+k}{\sqrt{3}}$. Though there is no any mathematical reason to use such a value for μ, the choice coincides with the gray plane on the RGB space with all three components equal.

The quaternion Fourier transform of type II is given by:

$$\boldsymbol{Q(k_x, k_y)} = \iint_{-\infty-\infty}^{\infty\infty} \boldsymbol{e^{-j2\pi k_x x)}\, h(x, y) e^{-k2\pi k_y y}\, dx\, dy} \tag{5.14}$$

and inverse transform

$$\boldsymbol{h(x, y)} = \boldsymbol{\frac{1}{4\pi^2}} \iint_{-\infty-\infty}^{\infty\infty} \boldsymbol{e^{j2\pi k_x x}\, Q(k_x, k_y) e^{k2\pi k_y y}\, dk_x dk_y} \tag{5.15}$$

The type I QFT can actually be considered as a generalization of the standard complex Fourier transform and hence shares some common properties. The main advantage of the quaternion Fourier transforms is their ability to transform a color image without the need for separating it into different color bands. For each spectral point the quaternion Fourier transform offers four component wave

number domain information rather than the six components we get from the standard complex Fourier transform of the color image as separate monochromatic components. This demonstrates a substantial saving of data storage. For RGB type of color image we can somehow relate the Eigen angle (phase), the Eigen axis and the modulus (amplitude) of the transform with the three color attributes: the hue, saturation and intensity of the image in the HSL space. This allows us to study all the color components and the correlation between them.

The quaternion Fourier transform has several applications. The standard auto and cross correlation definitions can be extended to color images using the quaternion Fourier transform. The quaternion Fourier transform has also interesting applications in localized color image analysis [68].

### 5.6.2. Trinion Principles and Trinion Fourier Transforms

A trinion number is defined with one real and two imaginary components as [2]:

$$t = a + ib + jc \tag{5.16}$$

where a, b and c are real numbers and i and j satisfy $i^2 = j$, $ij = ji = -1$ and $j^2 = -i$, and as opposed to quaternions, with these basis structures, trinions form a commutative ring. It is easy to show that all field axioms are satisfied by trinions but invertibility does not hold. That means trinions are not fields.

#### I. Some properties of Trinions

1. If $t_1 = a_1 + ib_1 + jc_1$ and $t_2 = a_2 + ib_2 + jc_2$ are two trinion numbers then addition and multiplication on $t_1$ and $t_2$ is defined very analogous to the complex case [1,2,69].

$$t_1 + t_2 = (a_1 + a_2) + i(b_1 + b_2) + j(c_1 + c_2) \tag{5.17}$$

$$t_1t_2 = (a_1a_2 - b_1c_2 - c_1b_2) + i(a_1b_2 + b_1a_2 - c_1c_2) + j(a_1c_2 + b_1b_2 + c_1a_2)$$

2. Trinions are associative as well as distributive with respect to addition and multiplication.
3. Distinct from quaternions, trinions are commutative both under addition and multiplication.
4. Any trinion number t = a + Ib + jc can be expressed as sum of a real part and a vector part as t = S(t)+V (t) where S(t) = a is the real part and V (t) = ib + jc is the vector part.

5. Trinion exponentiation is rather complicated [69].

6. Any trinion t = a + ib + jc can be written in the form

$$t = |t|(\cos(\phi) + \mu\sin(\phi)) \tag{5.18}$$

where $|t|=\sqrt{a^2+b^2+c^2}$, $\mu = \frac{V(t)}{|V(t)|}$, and $\phi=\arctan\frac{|V(t)|}{S(t)}$, $0\le\phi\le\pi$ are the amplitude,eigen axis (modulus), and eigen angle (phase), respectively. When |t| = 1 we call t a unit trinion and when a = 0 we call it a pure trinion.

7. If t = a + ib + jc is a trinion then its conjugate t is given by a rather complicated expression [1,2,69].

$$\bar{t} = \frac{(a^2+b^2+c^2)}{(a^3-b^3+c^3+3abc)}\left(a^2+bc-i(c^2+ab)-j(ac-b^2)\right) \tag{5.19}$$

## II. The trinion Fourier transform

Defining a Fourier type of transform in the trinion space is somehow difficult. One of the reasons is the non-invertibility of trinions. Other challenges include finding a Euler type of formula (if one exists) for trinion exponentials and proving if De Moivre's formula is still applicable in the trinion space, which is not routine task. In particular, we need those properties satisfied when we want to define the inverse transform. Since trinion exponentiation is not simple, we cannot try defining our transform using an exponential kernel like the standard Fourier transform. For that reason, a different approach will be presented below.

### a. The trinion Fourier transform-type I

Definition: Let h(x, y) be a given trinion valued image function. Then the trinion Fourier transform [69] of type I and its inverse are given by:

$$\mathbf{T}(\mathbf{k_x},\mathbf{k_y}) = \int_{-\infty}^{\infty}\int_{-\infty}^{\infty} \mathbf{h}(\mathbf{x},\mathbf{y})\left(\cos(2\pi\mathbf{k_x}\mathbf{x}+2\pi\mathbf{k_y}\mathbf{y}) - \boldsymbol{\mu}_1 \mathbf{si\,n}(2\pi\mathbf{k_x}\mathbf{x}+2\pi\mathbf{k_y}\mathbf{y})\right)\mathbf{dxdy} \tag{5.20}$$

and its inverse given by

$$\mathbf{h}(\mathbf{x},\mathbf{y}) = \frac{\mathbf{1}}{\mathbf{4\pi^2}}\int_{-\infty}^{\infty}\int_{-\infty}^{\infty} \mathbf{T}(\mathbf{k_x},\mathbf{k_y})(\cos(2\pi\mathbf{k_x}\mathbf{x}+2\pi\mathbf{k_y}\mathbf{y}) + \boldsymbol{\mu}_2 \sin(2\pi\mathbf{k_x}\mathbf{x}+2\pi\mathbf{k_y}\mathbf{y}))\,\mathbf{dk_x dk_y} \tag{5.21}$$

where $\boldsymbol{\mu_1}$ ***and*** $\boldsymbol{\mu_2}$ are unit trinions such that $\boldsymbol{\mu_1\mu_2}$ = -1. The choice of $\boldsymbol{\mu_1}$ ***and*** $\boldsymbol{\mu_2}$ is arbitrary as long as the product between them is -1.

## b. The trinion Fourier transform-type II

We can also define the trinion Fourier transform in other way [1,2].

Definition: Let h(x , y) be a given trinion valued image function. Then the trinion Fourier transform of type II and its inverse can be defined as:

$$\mathbf{T_2(k_x, k_y)} = \iint_{-\infty-\infty}^{\infty\infty} \mathbf{h(x,y)\,(\cos(2\pi k_x x) - \mu_1 \sin(+2\pi k_y y))(\cos(2\pi k_y y) - \mu_2 \sin(2\pi k_y y))dxdy} \tag{5.22}$$

and its inverse given by

$$\mathbf{h(X,Y)} = \frac{\mathbf{1}}{\mathbf{4\pi^2}} \iint_{-\infty-\infty}^{\infty\infty} \mathbf{T_2(x,y)(\cos(2\pi k_x x) + \mu_3 \sin(+2\pi k_y y))(\cos(2\pi k_y y) + \mu_4 \sin(2\pi k_y y))dxdy} \tag{5.23}$$

where $\mu_1$, $\mu_2$, $\mu_3$, $\mu_4$ are unit trinions satisfying $\mu_1\mu_3 = -1 = \mu_2\mu_4$.

In the above definition the choice of $\boldsymbol{\mu_1}$, $\boldsymbol{\mu_2}$, $\boldsymbol{\mu_3}$, $\boldsymbol{\mu_4}$ is again arbitrary. The simplest choice would be $\mu_1 = \mu_4 = i$ and $\mu_2 = \mu_4 = j$. The image function h(x, y) is the inverse of its trinion Fourier transform $T(k_x, k_y)$ of type II.

### 5.6.3. Comparing Trinion and Quaternion Based Formulations for Color Analysis

We have said that the trinion and the quaternion formulations of color image processing are holistic and much superior compared to the traditional monochromatic/serial analysis making use of the complex Fourier transform. Any color may be represented in terms of three components (RGB or HSL) or four components (CMYK). For the four component color representation the use of quaternions, with one real and three imaginary components, is natural. By setting one component to zero, quaternions have been used in RGB or HSL representation of colors and color images. Whereas trinions, with one real and two imaginary components, have significant efficiencies in representation, analysis and computation and are preferable for combined analysis of three component color images rather than separate monochromatic analysis of each component and use of quaternions [33]. As most color images have three components, the extra fourth dimension in quaternions creates redundancy. The three component trinions should be best suited to analyze such images. However, it must be mentioned that certain (algebraic) properties of trinions (such as exponentiation and inverse when it exists) are considerably more complicated compared to their counterparts in the natural complex and quaternion spaces [69].

## 5.7. The Proposed Algorithm

The proposed approach implemented both in the quaternion and the trinion spaces proceeds as follows.

1. First for every scan, the T1W, T2-FLAIR, and the ADC/PD images were combined to form a RGB color image. These trios were available MR parameters co-registered and ready for multi-parametric analysis.

- In the quaternion space, a RGB color image is written as a pure quaternion as:

$$h(x, y) = iR(x, y) + jG(x, y) + kB(x, y) \quad (5.24)$$

- In the trinion space, a RGB color image can uniquely be written as:

$$h(x, y) = R(x, y) + iG(x, y) + jB(x, y) \quad (5.25)$$

Note that the order of the mapping of a RGB image into a trinion does not affect the analysis as seen in previous studies [1,2,69].

2. Then each component is normalized to its maximum.
3. The (normalized) RGB image is then transformed to the HSL color space and the resulting color image is mapped as a trinion/quaternion. The usual RGB to HSL conversion was carried out in this case.
4. A spatially localized trinion/quaternion Fourier transform was then carried out on the resulting image.
5. Vectorial PCA analysis was then carried out.
6. Finally, higher order Haralick features were computed locally to generate a color signature map.

## Algorithm Flow Chart

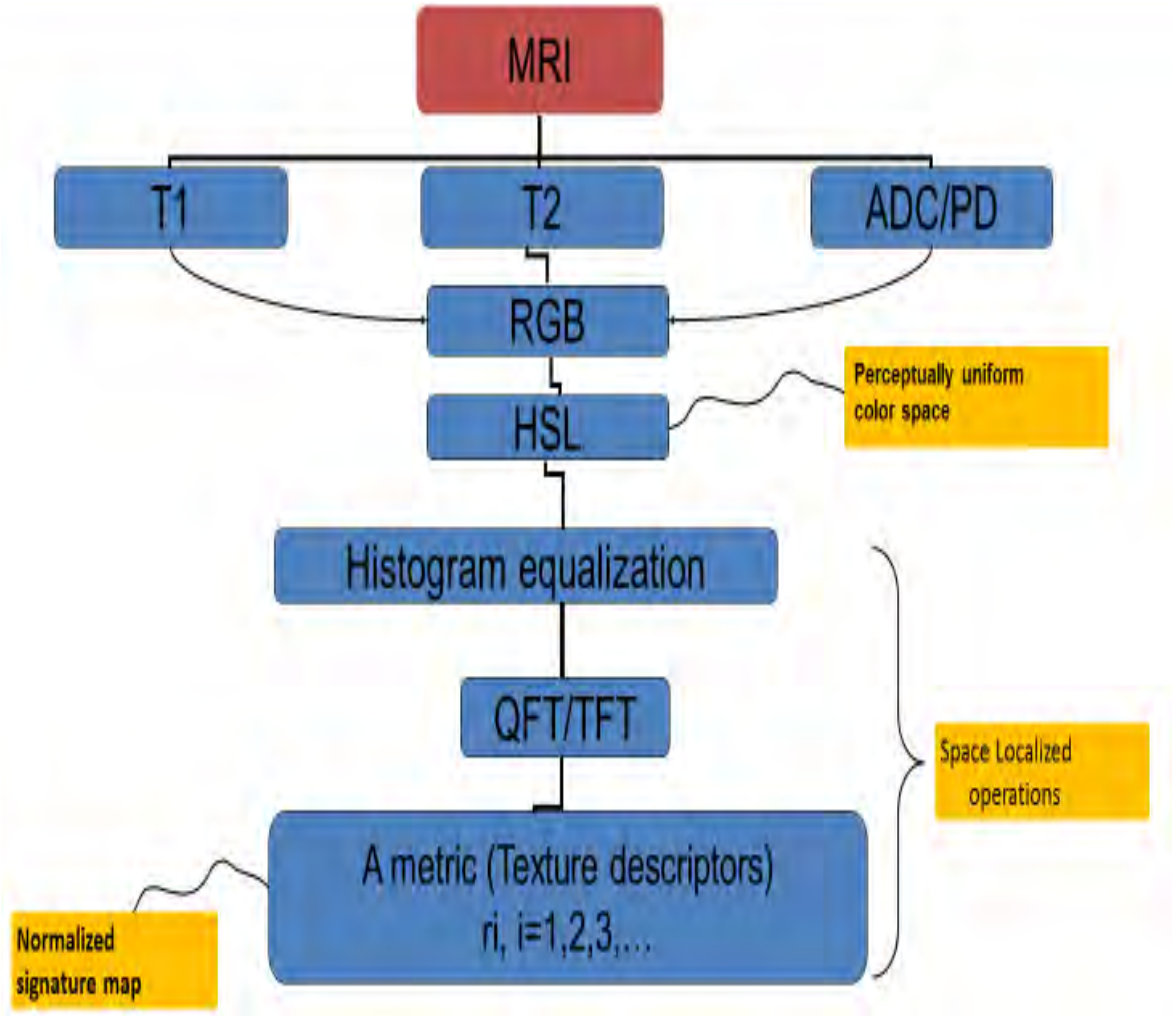

It is this map that has been used for tumor identification/detection/segmentation. These features, however, were Haralick only in form, i.e. use the same formula as Haralick to compute the features. The probability distribution functions ($p_{ij}$) that are used to compute Haralick features are derived from the Gray Level Co-occurrence Matrix (GLCM). But in the proposed method, the features are computed from probability distribution functions derived from the locally computed trinion/quaternion Fourier transforms followed by the application of a Vectorial version of PCA previously proposed in the literature on the 'algorito' website: (http://algorito.com/algorithm/principalcomponent-analysis-pca-transform).
Some of the features computed and the respective formulas (sum-mean, square-mean, variance, energy, entropy, etc.) are listed below:

$$Sum - mean_e = 0.5 \sum_{a=1}^{3} \sum_{b=1}^{3} (ap_{e_{ab}} + bp_{e_{ab}}) \quad (5.26)$$

$$Square - mean_e = 0.5 \sum_{a=1}^{3} \sum_{b=1}^{3} (ap_{e_{ab}}^2 + bp_{e_{ab}}^2) \quad (5.27)$$

$$Variance_e = 0.5 \sum_{a=1}^{3} \sum_{b=1}^{3} (a - M)^2 \, p_{e_{ab}} + (b - M)^2 p_{e_{ab}} \quad (5.28)$$

$$Energy(Angular\ second\ moment)_e = \sum_{a=1}^{3} \sum_{b=1}^{3} p_{e_{ab}}^2 \quad (5.29)$$

$$Entropy_e = \sum_{a=1}^{3} \sum_{b=1}^{3} p_{e_{ab}} \log(p_{e_{ab}}) \quad (5.30)$$

for e ∈ { 1, 2, 3, 4 }in the quaternion space ($e\epsilon\{1,2,3\}$, in the trinion spaces) and $M$ is the mean value of $p_{e.}$ Note that before computing the Haralick features $r_e$, we first rescaled the PCA entries $p_e$ in the range 0 to 1. The resulting quaternion $r_1 + r_2 i + r_3 j + r_4 k$ (trinion $r_1 + r_2 i + r_3 j$) was then assigned to the central voxel in that specific window. The step is then repeated across all voxels that are included in the selected region of interest (ROI). The final image (signature map) was generated as a color using the quaternion (trinion) valued local statistical features. Only the vector part is used to generate the quaternion signature map. In contrast, the trinion formulation allows us to image the whole signature map using both the

real and imaginary components of the trinion, and this is considered one significant advantage of the trinion formulation over the quaternion equivalent. Note that we used the fast Fourier transform (FFT) to compute both the QFT and the TFT very easily while development of standalone fast algorithms for the computation of both is beyond the scope of this thesis work.

The image sets used in this study were the ones used in a previous study [71] and were taken from a cohort of 29 patients treated for glioblastoma multiform(GBM) on a 1.5T MRI machine. Contrast-enhanced T1W gradient-echo and T2-FLAIR spin-echo as well as DWI MRIs of the patients acquired before, during, and after-radiation therapy were available for analysis. For each patient, all serial MR volumes were registered to the orientation of the baselineT1W image volume using the normalized mutual information algorithm and re-sampled to a common resolution using trilinear interpolation. The most important question we want to address using our scheme is how capable we are in automatically detecting different tissues, specifically diseases (GBM tumors) and normal structures, making a clever use of the enormous amount of information available within our MR multiple parameters. An expert radiation oncologist delineated the GTV corresponding to the contrast-enhancing lesion identified on the T1- weighted FSPGR images after IV administration of gadolinium DTPA contrast. For each patient, all serial MR volumes were registered to the orientation of the baseline T1W image volume using the normalized mutual information algorithm and re-sampled to a common resolution using trilinear interpolation. After performing rigid registration based on a mutual information metric, all contours were applied to the T2-FLAIR image and the ADC image sets.

# Chapter 6. Results and Discussion

Generally, the proposed scheme in this study that uses a vectorial color image processing concept and implemented in MATLAB to analyze multi-parametric MR images of patients treated for high grade brain tumor (GBM) has shown promising results. Following rigorous testing on the available data, the square mean 'Haralick' feature was found to be robust and more accurate in detecting the GBM tumors taken from the data set used in the thesis project. This comparison was preformed following a qualitative review of the generated signature maps and by comparing against the available ground truth information. The results showed that the method can effectively be used in automated GBM tumor identification when compared against the gold standard used in this study which, as mentioned before, is composed of the manual delineations by the expert radiologist. At this stage only qualitative analysis has been implemented and quantitative analysis will follow once complete segmentation scheme is developed. The detection scheme derived in this study is considered a very vital step towards effective segmentation.

There are some issues that must be mentioned before showing results of the application of the proposed scheme in detecting GBM tumors on the MP-MRI data set. Primarily the three MRI parameters considered (T1W, T2-FLAIR, and ADC) were taken with different resolution and the slice thicknesses and distance between slices were different. As a result, there was a need to apply co-registration and interpolation to bring the multiple parameters to a common resolution. There are usually inevitable registration inaccuracies in this regard which might considerably affect our analysis. The other issue is to do with the ground truth which was primarily derived based on a visual analysis by the expert which is prone to subjectivity. These and similar other issues pose challenges when implementing our scheme.

Figures 6.1, 6.2 and 6.3 present signature map results for three distinct patients with confirmed GBM (showing T1W, T2-FLAIR, and ADC original images followed by the combined color images as well as the corresponding signature maps). The

red lines on the signature maps indicate tumor delineations manually drawn by an expert radiation oncologist based on contrast enhanced T1W images.

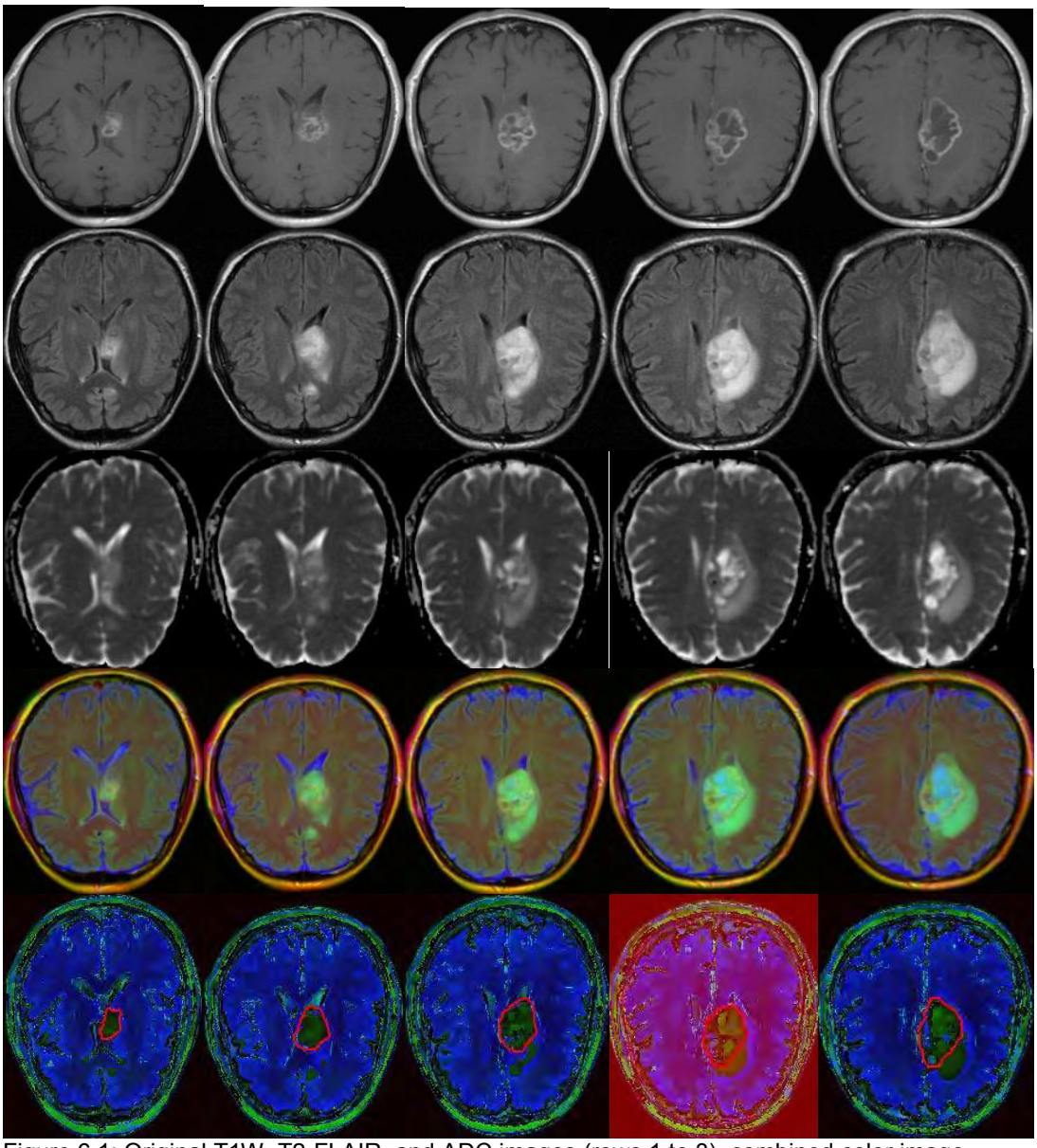

Figure 6.1: Original T1W, T2-FLAIR, and ADC images (rows 1 to 3), combined color image (row 4), and generated signature map (row 5). Red Lines denote the expert tumor delineations.

As shown in the Fig. 6.1, particularly for the first three MRI slices, there is a very good agreement between the tumor signatures (the greenish regions on the signature maps) and that of the radiologist's contour, with the exception of few outliers.

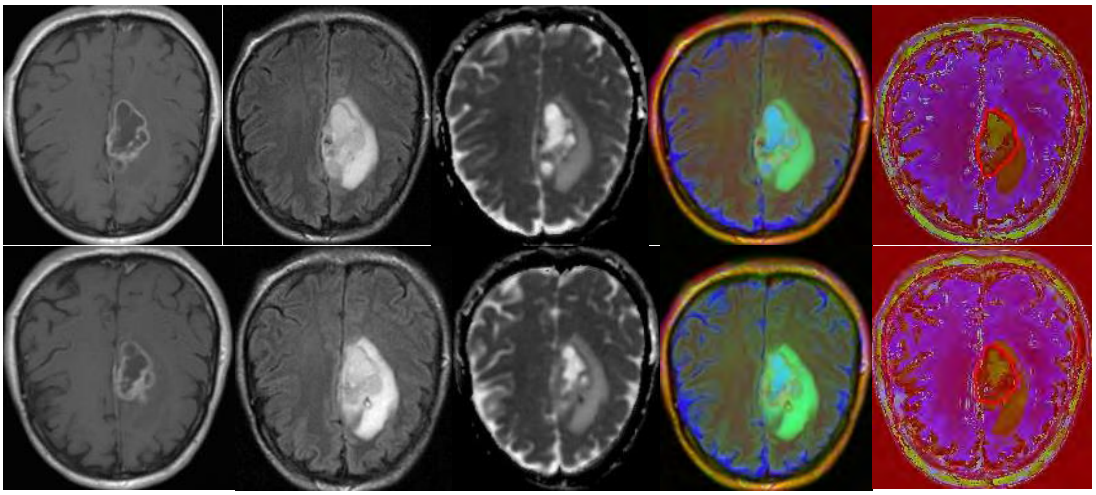

Figure 6.2: Original T1W, T2-FLAIR, and ADC images (column 1 to 3), combined color image (column 4), and generated signature map (column 5). Red Lines denote the expert tumor delineations.

For the following two MRI slices, however, the signature maps generated tend to cover more area outside the respective contours by the expert physician. Such differences are expected between the manual contours and that of the signature maps. Previous studies have shown that manual delineation of tumors based on different MR parameters is found to be very subjective [1, 2] and hence, as opposed to relying only on a single MRI parameter for manual tumor region delineation, the proposed scheme tries to automate the process making use of the combined multiple MR parameters to generate the signature maps using a suitable mathematical setup.

The signature map results for the second patient shown in Fig. 6.2 appears to over-fit the contours by the expert which as shown with the red lines. Figure 6.3 presents a case where the GBM tumor appears close to the skull boundary, which is often more challenging. The algorithm performed quit satisfactorily in detecting the GBM tumors in the different slices in this case too.

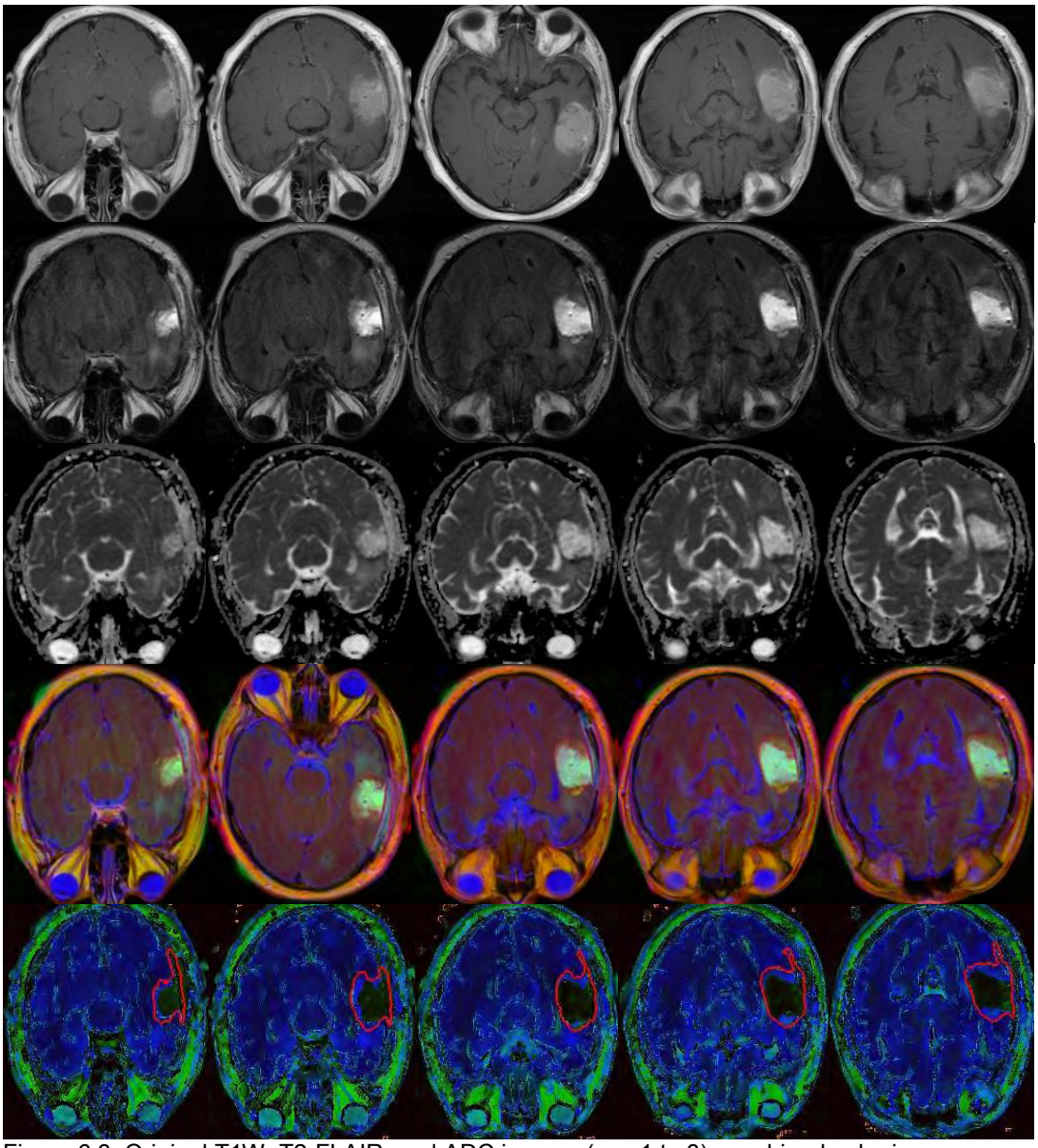

Figure 6.3: Original T1W, T2-FLAIR, and ADC images (row 1 to 3), combined color image (row 4), and generated signature map (row 5). Red lines denote the expert tumor delineations.

Figure 6.4 and 6.5 both present examples of signature maps generated for MRI slices with no GBM, which are used as controls in this thesis work. As expected no greenish signature is seen inside the brain tissue on the generated signature maps showing the robustness of the proposed scheme.

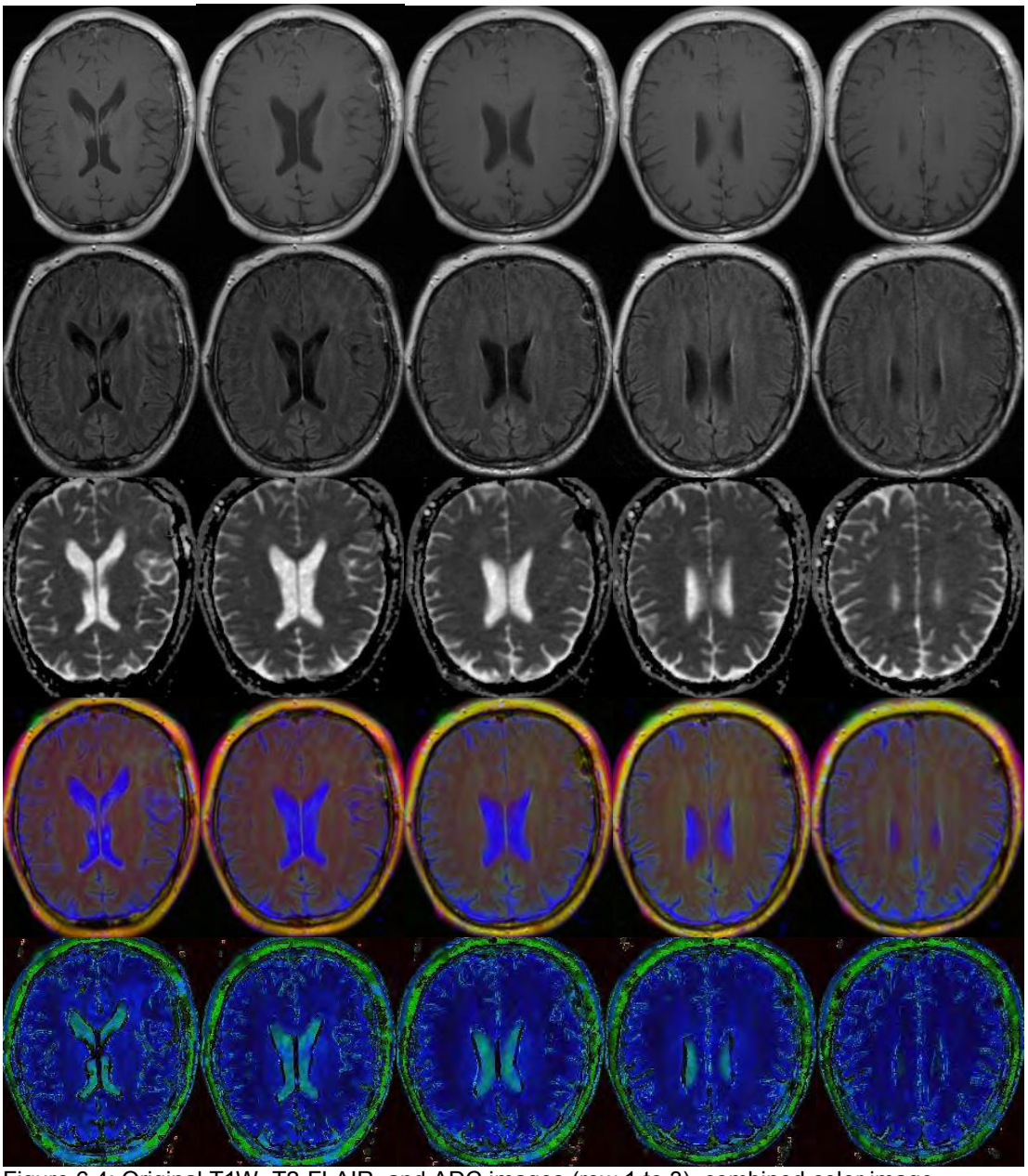

Figure 6.4: Original T1W, T2-FLAIR, and ADC images (row 1 to 3), combined color image (row 4), and generated signature map (row 5).

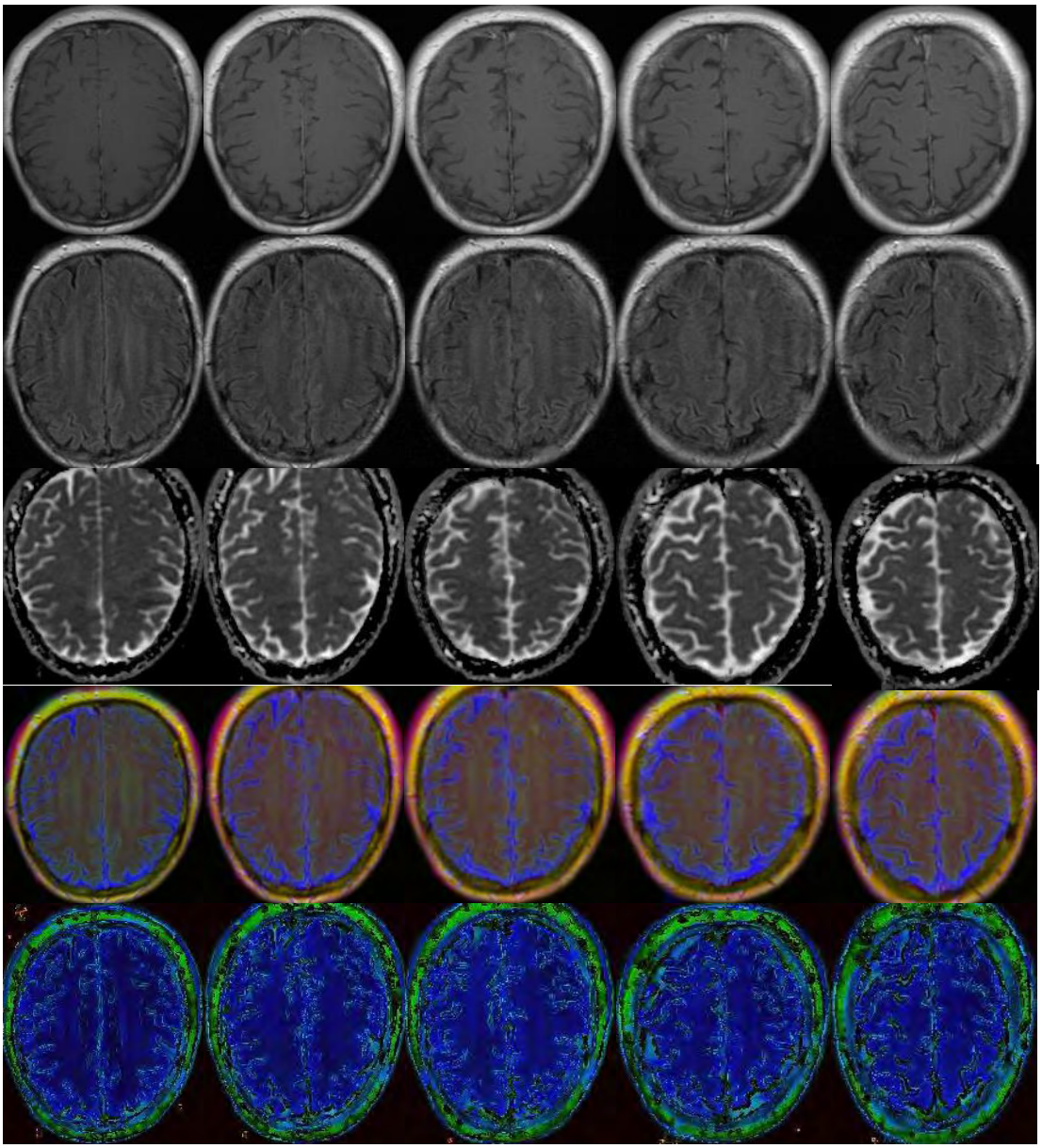

Figure 6.5: Original T1W, T2-FLAIR, and ADC images (row 1 to 3), combined color image (row 4), and generated signature map (row 5).

Though it is not presented in this thesis, the results found in the quaternion space were very similar to the ones computed in the trinion space despite the fact that the two spaces and their respective Fourier transforms are completely distinct. This is not totally unexpected as this is a holistic signal analysis we are implementing on the MP-MRI's and results should not entirely vary from one implementation space to the other (i.e. between quaternion and trinion spaces in our case).

All single parameter MR images were of size 256 x 256 pixels and when implemented in MATLAB a typical run takes about 25 seconds in the quaternion space and 20 seconds in the trinion space to compute a single signature map. This computation is significantly cheaper compared to most other implementations in the literature that use learned algorithms for example (Neural Networks, Genetic Algorithm, and the like). Note that at this testing phase, no effort has been exerted to make the MATLAB implementation more efficient which could significantly speed-up the computation. Actual implementations could only run in fractions of seconds making the proposed scheme to be useful in real time applications.

# Chapter 7. Conclusion and Future Directions

## 7.1. Conclusions

Ample literature has been reviewed in this thesis to describe different imaging modalities used in different applications of biomedicine. The focus was however on MRIs. Their origin, components, functionalities and related topics are thoroughly discussed. Particularly their use in generating multiple image parameters for use in multi-parametric studies is addressed.

Innovative approach is newly developed for use in cancer tissue detection and characterization based on multi-parametric MR images taken from patients treated for the highest grade glioma, glioblastoma multiform (GBM). Three MRI parameters of the brain were taken from the GBM patients and were combined as colors represented in a useful color space. The trios are holistically represented as color pixels in the trinion space and trinion based Fourier transforms are applied for further analysis of the pixels. Serial analysis of such multi component images pose a major challenge in that the inter correlation information that is embedded among the components could be missed which often carries a very useful information. Hence, a holistic and robust algorithm is designed and implemented in analyzing the multi-parametric MR images as multi-component colors and that goes much beyond what can be achieved by using any single parameter. The performance of the proposed algorithm is evaluated using images taken from a cohort of patients with confirmed GBM tumors in order to investigate its versatility and its suitability for usage in a clinical environment. The automated tool enabled differentiation of tumors from the surrounding normal brain tissue structures and the performance proved the fact that a holistic combination of the MR imaging parameters using the color concept is very useful compared to serial analysis of the different parameters. This could relive physicians from time consuming and subjective manual assessment, non-repetitive procedures and also possible observer variabilities.

Local analysis of multi-parametric MR images based on trinion based Fourier transform and the application of principal component analysis have resulted in

extraction of meaningful and robust features/descriptors for the cancer detection purpose. Different higher order features (having similar forms as that of the Haralick features) were computed and tested for their efficiency and one particular feature, namely the square mean feature, offered superior information than the rest of the features. This conclusion was derived, however, only as a result of qualitative assessment of the proposed method which is the intent and scope of the present study. A more quantitative assessment is still a work in progress.

The performance of the trinion (and also the quaternion) based schemes in GBM tumor identification was promising and can have a long-standing solution in the scientific and clinical armamentaria for assessing and understanding the nature and depth of brain tumor diseases. In general, there is a good agreement between the signature maps generated to signify the cancerous tumors and the available ground truth as drawn by an expert. Consequently, the proposed multi-channel image feature map can be used as a powerful tool for further GBM analysis purposes. Moreover, this framework has potential benefits to make effective predictions on the nature of GBM exclusively. With further research, a system could be developed on different data sets and may be useful for further validation to investigate potential clinical implications for patients. Ongoing research focuses on the enhancement of the detection algorithm, development of a complete segmentation scheme and a more quantitative evaluation of the method accompanied by clinical validation.

This report also aids as a proof of concept that MR imaging offers much useful information compared to other imaging modalities due to its flexibility for structural, functional and metabolic measurements, particularly in the case of the brain.

## 7.2. Future Directions

Only qualitative analysis of the results is presented in this study while quantitative analysis (against the gold standard) awaits complete segmentation of the tumors. The complete segmentation of the detected GBM tumors will require designing a classification scheme. There are already various classification schemes available in the literature which can use the signature map results as inputs. It could be said

that the signature maps and features which could be derived from it are clever inputs which can be used towards complete segmentation of the tumors.

In principle, other than the MP-MRI images, the proposed scheme can be applied to other color medical images generated with different modalities. That by no means should imply that the same algorithm can be used in analyzing any given medical image with multiple parameters/channels/bands. However, a similar scheme can be applied to extract robust higher order features which can be used in detection of objects of interest on the respective medical images.

Many potential clinical implications of the results by the proposed scheme can be mentioned. One could be for an easy location of gross tumor volumes (GTVs) for use in optimal delivery of radiation treatment. Also the features could be checked for their usability as biomarkers for quantifying patients' treatment response(survival, disease progression and other known end-points). More important clinical evaluations of the proposed scheme must be checked thoroughly through a rigorous observer study.

In the first long-term view, we will need to put our focus over the local MR image data which could be obtained from Mekelle University, Ayider Referal Hospital, Addis Ababa University Health Science college of Black Lion Specialized Hospital, Jimma University Hospita and other private and governmental health institutions. The local data accessed from data bases found at the Mekelle Ayider Referal Hospital and Yehulushet H. Clinic were only used for testing and validation (proof of concept) purposes as those data lacked strict ground truth information. Furthermore data obtained from patients in a certain cohort are preferred than arbitrary MR images taken from arbitrary patients. Undoubtedly, it awaits much further research before some of the results found in this thesis project could actually be translated to the clinics.

**References:**


1. Dawit Assefa, Harry Keller, and David A. Jaffray; Signal Analysis of Multi-parametric MR Images in Higher Order Fourier Spaces, International Journal of Computational Bioscience, Vol. 4, No. 1, 2013.
2. Dawit Assefa, Harry Keller and David A.Jaffray; Multi-parametric MR Imaging Processing Using Higher Dimensional Vector Algebra, ACTA press, IASTED/ISPHT, pp. 24-31, DC, US, May 2011.
3. Deanna Lyn Langer; Multi-parametric Magnetic Resonance Imaging (MRI) in Prostate Cancer, 2010
4. Volker Baecker; volker.baecker@mri.cnrs.fr; http://rsb.info.nih.gov/ij/. Image Processing and Analysis with Image J and MRI Cell Image Analyzer Montpellier RIO Imaging; 30/04/2010;
5. Geoffrey S. Young; Advanced MRI of Adult Brain Tumorsa Department of Radiology, USA; June 2010.
6. Rajan T. Gupta, Christopher R. Kauffman, Thomas J. Polascik, FACS2, Samir S. Taneja, Andrew B. Rosenkrantz; Update on Brain Tumor Imaging: From Anatomy to Physiology; April 15, 2013;
7. Benjamin Lemasson, Thomas Christen, Xavier Tizon, Régine Farion, Nadège Fondraz Peggy Provent, Christoph Segebarth, Emmanuel L. Barbier, Philippe Genn, Olivier Duchamp, Chantal Remy; Assessment of Multi-parametric MRI in a Human Glioma Model to Monitor Cytotoxic and Anti-angiogenic drug effects; 2008.
8. University of California, San Franscisco, The state of prostate cancer in 2013; Department of Radiology and Neurological surgery, April 2013.
9. Ragini Verma, Evangelia I., Zacharaki, YangmingOu, HongminCai, Sanjeev Chawla, Seung-Koo Lee,Elias R. Melhem, Ronald Wolf, Christos Davatzikos; Multiparametric Tissue Characterization of Brain Neoplasms and Their Recurrence Using Pattern Classification of MR Images; May 2011.
10. Blackwell Publishing Company: Director of Training and Education Lodestone Patient Care Ltd; MRI at a Glance Catherine Westbrook 9600 Garsington Rd, Oxford OX4 2DQ, UK, 2005.

11. Firoz Ahmed, Shahnaz Rahman, Nasir Ahmed, Maraz Hossain, Anup Biswas, Sanjoy Sarkar, Hasanul Banna, Afsana Khatun, Majeedul H. Chowdhury, Mohammed Rahmatullah; Image Features analysis and segmentation; 2011.
12. Lothar Schad, Physics of Systems (ROE, CT, MRI), 2008.
13. Juan Eugenio Iglesias, Ender Konukoglu, Darko Zikic, Ben Glocker, Koen Van Leemput and Bruce Fischl, Is Synthesizing MRI Contrast Useful for Inter-modality Analysis?, 2013.
14. Anwar Padhani, Multiparametric Imaging of Tumors – an Emerging Paradigm, 29/03/2014
15. Michael A. Jacobs, Zheng G. Zhang, Robert A. Knight, Hamid Soltanian-Zadeh, Anton V., Goussev, Donald J. Peck and Michael Chopp, A Model for Multiparametric MRI Tissue Characterization in Experimental Cerebral Ischemia With Histological Validation in Rat: Part 1, 2014
16. E. Mandonnet, Capelle, L. and U. Duffau, 'Extension of paralimbic low grade gliomas: toward an anatomical detection based on white matter invasion patterns', 2009.
17. Anthea Wright, Brain scanning techniques (CT, MRI, fMRI, PET, SPECT, DTI, DOT), Cerebra, 2010.
18. A. Michotte, B. Neyns, C. Chaskis, et.al, 'Neuropathological and molecular aspects of low-grade and high grade gliomas', 2011.
19. M. Essig,. N. Anzalone, S. E. Combs, et.al, 'Imaging of Neoplastic Central Nervous System Lesions', 2012.
20. W. Bian, S. K Inas , M. L. Janine et.al, 'Multiparametric Characterization of Grade 2 Glioma using magnetic Resonance Spectroscopic, perfusion, and Diffusion Imaging', 2009.
21. Suzanne Laughlin, FRCPC; Walter Montanera, FRCPC VOL 104 / NO 5 / November 1998 / Postgraduate Medicine, "Central nervous system imaging When is CT more appropriate than MRI?", 1998
22. Antonio Di Ieva, Fractal Analysis of Micro-vascular Networks in Malignant Brain Tumors, 4/3/2014

23. David Manuel Galaz Tavares, MRI/TRUS data fusion Prostate cancer diagnostic and focal treatment, October 201
24. N. Behzadfar and H. Soltanian-zadeh; Reproducibility Study of Prediction of Brain Tumors Response to Bevacizumab Treatment, March, 2014.
25. Elda Fischi G ´omez et.al, Inhomogeneity Correction in High Field Magnetic Resonance Images: Human Brain Imaging at 7 Tesla, July 2008.
26. Evert J Blink, MRI : Physics, November, 2004
27. Kari Mäkelä, BME, TUTBasics of MRI, 2011.
28. Design and Optimisation of Radio-Frequency Probes for High Field Magnetic Imaging by Amany Ali Alsuraihi, 2011
29. William R. Hendee, E. Russell Ritenour; Medical Imaging Physics Fourth Edition, 2008
30. Hashemi, Ray Hashman; Bradley, William G.; Lisanti, Christopher J. Lippincott Williams & Wilkins, MRI: The Basics, 2nd Edition
31. Multi-parametric Magnetic resonance imaging from Wikipedia, the free encyclopedia Jump to: navigation, search: http://www.tele.ucl.ac.be/ PEOPLE/OC/the.
32. Assaf Tal, Basic Spin Physics, 30/10/2012
33. Kathryn M. McMillan, Baxter P. Rogers, Cheng Guan Koay, Angela R. Laird, Ronald R. Price, M. Elizabeth Meyerand; An objective method for combining multi-parametric MRI datasets to characterize malignant tumors, January 2010
34. Mona Choubey and Suyash Agrawal; A Fully Automatic Approach to Detect Brain Cancer Using Random Walk Algorithm; Jan-Feb, 2012
35. By Rajan T. Gupta, Christopher R. Kauffman, Thomas J. Polascik, FACS2, Samir S. Taneja, Andrew B. Rosenkrantz; Update on Brain Tumor Imaging: From Anatomy to Physiology; April 15, 2013.
36. Andrea Sbarbati and Marzola a; Advanced image-processing techniques in magnetic resonance imaging for the investigation of brain pathologies and tumour angiogenesis, 2011.
37. Ray Maleh, Efficient Sparse Approximation Methods for Medical Imaging; May 2011.

38. Philippe Bolon, Marlène Wiart, Ludovic Macaire, Pierre Gouton, Thomas Grenier, Hugues Benoit-Cattin; Contributions to Mean Shift filtering and segmentation, Applications to MRI ischemic data, 2012
39. N. Gopinath, Extraction of Cancer Cells from MRI Brain Image Using MATLAB, International Journal of Engineering Science and Innovative Technology (IJESIT) Volume 1, Issue 1, September 2012.
40. Juan Eugenio Iglesias, Ender Konukoglu, Darko Zikic, Ben Glocker, Koen Van Leemput and Bruce Fischl; Is Synthesizing MRI Contrast Useful for Inter-Modality Analysis?, 2011.
41. Paul M. Parizel , Luc van den Hauwe , Frank De Belder , J. Van Goethem Caroline Venstermans , Rodrigo Salgado , Maurits Voormolen , and Wim Van Hecke, Magnetic Resonance Imaging of the Brain, 2009
42. T. M . Deserno, Biomedical Image Processing, Biological and Medical Physics, Biomedical Engineering, DOI: Springer-Verlag Berlin Heidelberg; 2011
43. Kari Mäkelä BME, TUT; Basic MR imaging Tissue Signal Characteristics, 2011
44. Indra Dev Sahu, Sheshkant Aryal, Shanta Lal Shrestha, Ram Kumar Ghimire; Comparison of Fluid Attenuated Inversion Recovery Sequence with Spin Echo T2-Weighted MRI for Characterization of Brain Pathology; 2010
45. Shuda Chen, Fusao Ikawa, Kaoru Kurisu, Katsunori Arita, Junko Takaba, and Yukari Kanou; Quantitative MR Evaluation of Intracranial Epidermoid Tumors by Fast Fluid-attenuated Inversion Recovery Imaging and Echo-planar Diffusion-weighted Imaging; June/July 2007
46. Majda M. Thurnher, Siegfried A. Thurnher, Dominik Fleischmann, Andrea Steuer, Armin Rieger, Thomas Helbich, Siegfried Trattnig, Erwin Schindler, and Karl Hittmair Comparison of T2-Weighted and Fluid-Attenuated Inversion-Recovery Fast Spin-Echo MR Sequences in Intracerebral AIDS-Associated Disease; 18, October 1997
47. Vincent P. Mathews; Karen S. Caldemeyer,; Mark J. Lowe; Stacy L. Greenspan; DO David M. Weber, PhD; John L. Ulmer; Brain: Gadolinium-enhanced Fast Fluid-attenuated Inversion-Recovery MR Imaging; 1999.

48. Okechukwu Felix Erondu; Medical Imaging, 2011.
49. Joseph Bronzino, Richard A.Robb, Ranjaraj M. Rangayyan, H.K. Huang; Hand book of Medical Imaging, processing and analysis, 2011.
50. K. M. M. Rao, V. D. P. Rao; Medical Image Processing, 2009.
51. Peter B. Cotton & Christopher B. Williams Practical Gastrointestinal Endoscopy Sixth edition; 2008.
52. S. Young, Department of Radiology, Brigham and Women's Hospital; Advanced MRI of Adult Brain Tumors Geoffrey, 2007.
53. L. Celso Hygino da Cruz Jr.; Emerson L. Gasparetto; Roberto C. Domingues; Romeu C.; Diffusion-Weighted MR Imaging in Brain Tumor, 2008.
54. Wei Bian, Inas S. Khayal, Janine M. Lupo, Colleen McGue, Scott Vandenberg, Kathleen R. Lamborn, Susan M. Chang, Soonmee Cha, and Sarah J. Nelso; Multiparametric Characterization of Grade two Glioma Subtypes Using Magnetic Resonance Spectroscopic, Perfusion, and Diffusion Imaging; December 2009.
55. Bauer Z., Roland Wiest, Lutz-P. Nolte, and Mauricio Reyes; A Survey of MRI-based Medical Image Analysis for Brain Tumor Studies Stefan, 2011
56. Caroline Chung; Imaging Biomarkers of Response to Radiation and Anti-angiogenic Agents in Brain Tumors; 2011.
57. B. D. Venkatramana Reddy and T. Jayachandra Prasad; Colour-Texture Image Segmentation using Hypercomplex Gabor Analysis; December 2010.
58. W. R. Hamilton (1866). Elements of Quaternions. London, U.K: Longmans Green.
59. E.B. Podgorsak, Technical Editor; Radiation Oncology Physics: A Handbook for Teachers and Students; International Atomic Energy Agency Vienna, 2005
60. E.B. Podgeorsak; Radiation physics for Medical Physicists, Biological and Medical physics Biomedical Engineering; 2009.
61. Health Physics Society Specialists in Radiation Safety (HPS); Radiation Exposure from Medical Exams and Procedures; January 2010.
62. Bharat Annaldas; Multi-parametric MRI Study of Brain Insults (*Traumatic Brain Injury and Brain Tumor*) in Animal Models; July 2014.

63. An International Journal (CSEIJ), Vol.1;Computer Science & Engineering: No.5;MRI image segmentation using level set method and implement a medical diagnosis system; December 2011.
64. Kassner and Thornhill;Image Features for Segmentation Algorithms; 2010
65. Tuceryan and Jain; Image Segmentation and Texture analysis; 1998.
66. Bjoem Andres, Ullrich Koeth, Thorben Kroeger, Moritz Helmstaedter, Kevin L. Briggman, Winfried Denk, Fred A. Hamprecht; Medical Image Analysis; 2012.
67. Laura S. Schmidt, Michael L. Nickerson, Michelle B. Warren, Gladys M. Glenn, Jorge R. Toro, Maria J. Merino, Maria L. Turner, Peter L. Choyke, Nirmala Sharma, James Peterson, Patrick Morrison, Eamonn R. Maher, McClellan M. Walther Berton Zbar, and W. Marston Linehan; Image Pattern Recognition and Segmentation Analysis; 2005
68. Dawit Assefa, L. Mansinha, K. F. Tiampo, H. Rasmussen, K. Abdella; Local quaternion Fourier transform and color image texture analysis, Signal processing; ; 90(6), pp.1825-1835, 2010.
69. Dawit Assefa, L. Mansinha, K. F. Tiampo, H. Rasmussen, K. Abdella; The trinion Fourier transform of color images, Signal processing; 91(8), pp. 1887-1900, 2011.
70. A. Materka, M. Strzelecki; Texture Analysis Methods – A Review,1998.
71. Dawit Assefa, H. Keller, C. M´enard, N. Laperriere, R. J. Ferrari, and I. Yeung, Robust texture features for response monitoring of glioblastoma multiforme on T1-weighted and T2-FLAIR MR images: a preliminary investigation in terms of identification and segmentation, Medical Physics, 37(4), 1722–1736, 2010.

APPENDIX: MATLAB Code Implementation

```
%Test classificaion - with trinions...
clear all
close all
clc
s_num = 24;
tic
R_comp_temp = analyze75read('C:\Users\Tefe-
defacto\Desktop\P8\P9_T1.img');
R_comp = (R_comp_temp(:,:,s_num));
w(:,:,1) = R_comp;
figure
imshow(R_comp_temp(:,:,s_num),[])
G_comp_temp = analyze75read('C:\Users\Tefe-
defacto\Desktop\P8\P9_T2.img');
G_comp = (G_comp_temp(:,:,s_num));
w(:,:,2) = G_comp;
figure
imshow(G_comp_temp(:,:,s_num),[])
B_comp_temp = analyze75read('C:\Users\Tefe-
defacto\Desktop\P8\P9_ADC.img');
B_comp = (B_comp_temp(:,:,s_num));
w(:,:,3) = B_comp;
figure
imshow(B_comp_temp(:,:,s_num),[])
w = double(w);
T_R = w(:,:,1);
T_G = w(:,:,2);
T_B = w(:,:,3);
w(:,:,1) = T_R;
w(:,:,2) = T_G;
w(:,:,3) = T_B
w_old(:,:,1) = double(w(:,:,1)./max(max(abs(w(:,:,1)))));
w_old(:,:,2) = double(w(:,:,2)./max(max(abs(w(:,:,2)))));
w_old(:,:,3) = double(w(:,:,3)./max(max(abs(w(:,:,3)))));
figure, imshow(double(w_old),[])
w_old(:,:,1) = adapthisteq(w_old(:,:,1));
w_old(:,:,2) = adapthisteq(w_old(:,:,2));
w(:,:,1) = w_old(:,:,1);
w(:,:,2) = w_old(:,:,2);
w(:,:,3) = w_old(:,:,3);
HHH = w(:,:,1);
SSS = w(:,:,2);
LLL = w(:,:,3);
FL = (HHH+SSS+LLL)/sqrt(3.0);
V_1 = (2.0*LLL-HHH-SSS)/sqrt(6.0);
V_2 = (HHH-SSS)/sqrt(2.0);
si = size(V_1);
FS = sqrt(V_1.^2+V_2.^2);
FH = (atan2(V_2,V_1));
FA = sqrt(HHH.^2+SSS.^2+LLL.^2);
FPHI = acos(FL./FA);
for qa_1 = 1:si(1)
    for qa_2 = 1:si(2)
        if (V_2(qa_1,qa_2) >= 0)
            if (V_1(qa_1,qa_2) >= 0)
```

```
                FH(qa_1,qa_2) = ((FH(qa_1,qa_2))./(2*pi)).^1;
            else
                FH(qa_1,qa_2) = ((FH(qa_1,qa_2))./(2*pi)).^1;
            end;
        else
            if (V_1(qa_1,qa_2) >= 0)
                FH(qa_1,qa_2) = ((FH(qa_1,qa_2))./(2*pi)).^1
            else
                FH(qa_1,qa_2) = ((FH(qa_1,qa_2))./(2*pi)).^1;
                %FH(qa_1,qa_2) = (abs(FH(qa_1,qa_2))./(2*pi)).^2;
            end;
        end;
    end;
end;
w(:,:,1) = abs(FH);
w(:,:,2) = FS;
w(:,:,3) = FL;
Te_1 = atan2(V_2,V_1);
Te_2 = (acos(FL./FA));
Te_3 = FA;
sz = size(w(:,:,1));
las_x = sz(1) - 2;
las_y = sz(2) - 2;
st_pt_x = 1;
st_pt_y = 1;
for r_s_x = 1:las_x
    for r_s_y = 1:las_y
trt = 1;
[L_1,L_2,L_3] = PH_trinion_typeI_non_localized(w(st_pt_x+r_s_x-
trt:st_pt_x+r_s_x+trt,...
   st_pt_y+r_s_y-trt:st_pt_y+r_s_y+trt,1),w(st_pt_x+r_s_x-
trt:st_pt_x+r_s_x+trt,...
   st_pt_y+r_s_y-trt:st_pt_y+r_s_y+trt,2),w(st_pt_x+r_s_x-
trt:st_pt_x+r_s_x+trt,...
   st_pt_y+r_s_y-trt:st_pt_y+r_s_y+trt,3));
[r_1,r_2,r_3] =
Vectorial_PCA_Transform_with_trinions(abs(L_1),abs(L_2),abs(L_3));
mi = min(min(min(r_1(:)),min(r_2(:))),min(r_3(:)));
if (min(r_1(:)) < 0)
        r_1 = r_1 + abs(mi);
end;
if (min(r_2(:)) < 0)
        r_2 = r_2 + abs(mi);
end;
if (min(r_3(:)) < 0)
        r_3 = r_3 + abs(mi);
end;
ma = max(max(max(abs(r_1(:))),max(abs(r_2(:)))),max(abs(r_3(:))));
mi = min(min(min(r_1(:)),min(r_2(:))),min(r_3(:)));
if(max(abs(r_1(:))) > 1)
         r_1 = r_1./ma;
end;
if(max(abs(r_2(:))) > 1)
         r_2 = r_2./ma;
end;
if(max(abs(r_3(:))) > 1)
         r_3 = r_3./ma;
```

```
end;
for z_1 = 1:3
    for z_2 = 1:3
         SM_1(z_1,z_2) = 0.5*double(z_1
(z_2).*r_1(z_1,z_2).^2;%0.5*(double(z_1) - mean(r_1(:))
         SM_2(z_1,z_2) = 0.5*double(z_1 +
z_2).*r_2(z_1,z_2).^2;%0.5*(double(z_1) - mean(r_2(:)))^2*r_2(z_1,z_2)
         SM_3(z_1,z_2) = 0.5*double(z_1 +
z_2).*r_3(z_1,z_2).^2;%0.5*(double(z_1) - mean(r_3(:)))^2*r_3(z_1,z_2)
    end;
end;
Summean_1 = sum(SM_1(:));
Summean_2 = sum(SM_2(:));
Summean_3 = sum(SM_3(:));
PCA_Q_Eax(r_s_x,r_s_y,1) = (Summean_1);%abs((Summean_3) -
PCA_Q_Eax(r_s_x,r_s_y,2) = (Summean_2);%abs((Summean_3) -
PCA_Q_Eax(r_s_x,r_s_y,3) = (Summean_3);%abs((Summean_2) -
clear L_1 L_2 L_3 r_1 r_2 r_3
    end;
end;
toc
if (max(max(abs(PCA_Q_Eax(:,:,1)))) ~= 0.0)
    PCA_Q_Eax(:,:,1) =
PCA_Q_Eax(:,:,1)./max(max(abs(PCA_Q_Eax(:,:,1))));
end;
if (max(max(abs(PCA_Q_Eax(:,:,2)))) ~= 0.0)
    PCA_Q_Eax(:,:,2) =
PCA_Q_Eax(:,:,2)./max(max(abs(PCA_Q_Eax(:,:,2))));
end;
if (max(max(abs(PCA_Q_Eax(:,:,3)))) ~= 0.0)
    PCA_Q_Eax(:,:,3) =
PCA_Q_Eax(:,:,3)./max(max(abs(PCA_Q_Eax(:,:,3))));
end;
W_Pow = w_old;
W_Pow(st_pt_x+1:st_pt_x+las_x,st_pt_y+1:st_pt_y+las_y,1) =
PCA_Q_Eax(:,:,1);
W_Pow(st_pt_x+1:st_pt_x+las_x,st_pt_y+1:st_pt_y+las_y,2) =
PCA_Q_Eax(:,:,2);
W_Pow(st_pt_x+1:st_pt_x+las_x,st_pt_y+1:st_pt_y+las_y,3) =
PCA_Q_Eax(:,:,3);
W_Pow = W_Pow./max(abs(W_Pow(:)));
alp = analyze75read('C:\Users\Tefe-defacto\Desktop\P8\P9_voi.img');
alp_new(:,:,1) = alp(:,:,s_num);
alp_new(:,:,2) = alp(:,:,s_num);
alp_new(:,:,3) = alp(:,:,s_num);
figure
imshow(W_Pow,[]), hold on
title('Full entropies as colors')
hold on
x_vec = double(0:255);
y_vec = double(0:255);
uo_1 = pi*sin(2*pi*x_vec(1:128)./400.0)'*sin(2*pi*y_vec(1:128)./400.0);
alpha = double(alp_new);
alpha = alpha./max(alpha(:));
[we_x we_y] = gradient(alpha(:,:,1));
[gx_1 gy_1] = find(we_x == max(we_x(:)));
[gx_2 gy_2] = find(we_x == min(we_x(:)));
```

```
[gx_3 gy_3] = find(we_y == max(we_y(:)));
[gx_4 gy_4] = find(we_y == min(we_y(:)));
plot(gy_1,gx_1,'r.','LineWidth',3,'MarkerEdgeColor','r','MarkerFaceColo
r','r','MarkerSize',3), hold on
plot(gy_2,gx_2,'r.','LineWidth',3,'MarkerEdgeColor','r','MarkerFaceColo
r','r','MarkerSize',3), hold on
plot(gy_3,gx_3,'r.','LineWidth',3,'MarkerEdgeColor','r','MarkerFaceColo
r','r','MarkerSize',3), hold on
plot(gy_4,gx_4,'r.','LineWidth',3,'MarkerEdgeColor','r','MarkerFaceColo
r','r','MarkerSize',3), hold off
```